7-20-2022

Wetland Soil Development Along Salinity and Hydrogeomorphic Gradients in Active and Inactive Deltaic Basins of Coastal Louisiana

Amanda Fontenot
Louisiana State University and Agricultural and Mechanical College

WETLAND SOIL DEVELOPMENT ALONG SALINITY AND HYDROGEOMORPHIC GRADIENTS IN ACTIVE AND INACTIVE DELTAIC BASINS OF COASTAL LOUISIANA

A Thesis

Submitted to the Graduate Faculty of the
Louisiana State University and
Agricultural and Mechanical College
in partial fulfillment of the
requirements for the degree of
Master of Science

in

The Department of Civil & Environmental Engineering

by
Amanda Marie Fontenot
B.S., Louisiana State University, 2018
August 2022

Acknowledgements

I would like to thank my advisors, Dr. Clint Willson and Dr. Robert Twilley, for their support and direction throughout this program. I would also like to thank Dr. John R. White, Dr. Tracy Quirk, and Dr. Navid Jafari for their patience, insightful questions, and service on my thesis committee. This master project was part of the National Aeronautics and Space Administraction's (NASA) Delta-X Mission. The NASA Delta-X project is funded by the Science Mission Directorate's Earth Science Division through the Earth Venture Suborbital-3 Program NNH17ZDA001N-EVS3. I am thankful for the opportunity to be a small part of this amazing team.

Thank you to Dr. Andre Rovai for his support and collaboration of this project from the very beginning. Thank you to Zoë Shribman for the constant words of encouragement and innumerable hours on the phone discussing this research – we did it! Thank you also to my amazing co-workers Denise Poveda, Alex Christensen, Song Li, Brandon Wolff, Danielle Soileau, Elizabeth Bogan, and John O'Connor for the training, field, and lab support. Thank you also to the student workers that helped process my samples. It truly was a team effort to get this project done, and I am eternally grateful for everyone's help.

I would also like to thank my friends for their continued physical and emotional support in my life. I couldn't have finished this without you all. Thank you to my spouse for holding my hand through this portion of my life and staying by my side on the good days and the bad. I'd also like to thank my father for encouraging me to start and stay in this program; I hope I have made you proud.

Table of Contents

List of Tables

List of Figures

Abstract

Coastal wetlands provide an abundance of ecosystem services that benefit society, such as essential habitat for commercial species, storm protection, nutrient cycling, and carbon storage. Louisiana faces rapid rates of relative sea level rise (natural subsidence and eustatic sea levels) that threaten wetland survival, which are amplified by a reduction of riverine sediment input. An important determining factor of marsh survival is the formation of wetland platform elevation, known as vertical accretion, which is determined by several processes including sediment deposition & erosion, below ground biomass (BGB) productivity, decomposition of organic matter, shallow & deep subsidence, and soil compaction. Feldspar marker horizon stations were deployed in an active (Atchafalaya Bay) and an inactive (Terrebonne Bay) coastal basin along salinity and hydrogeomorphic (HGM) zone gradients to quantify surface accretion in wetlands exposed to different loadings of riverine sediment. Surface accretion rates were greatest in Wax Lake Delta (3.5-5.7 cm yr^{-1}) in the proximal region of an active basin and lower in the distal region in Fourleague Bay brackish and saline marshes (1.42 cm yr^{-1}). In contrast, surface accretion and inorganic and organic sedimentation rates increased with increased salinity in the inactive Terrebonne Bay. Average BGB ranged from 600-5500 g m^{-2} while average total root mass ranged from 3000-11000 g m^{-2} for 50cm deep cores. Belowground necromass had increased lignin content and slower decomposition rates, suggesting necromass is an important component of soil formation.

Filed observations were used to parameterize the NUMAR model (numerical marsh accretion and response), a modification of the NUMAN (Chen and Twilley 1999) and SEMIDEC (Morris and Bowden 1986) models. NUMAR uses surface accretion rates, soil physicochemical characteristics of newly accreted material, and belowground biomass dynamics to estimate

decadal (70 yr) sediment accretion rates comparable to ^{137}Cs dated cores. NUMAR was calibrated across salinity gradients in two different coastal basins, however model development is needed to capture important soil building dynamics, such as soil compaction and interannual vertical accretion variability. This model will be applied to an ecogeomorphic landscape model of Atchafalaya and Terrebonne and can help inform wetland restoration and management of coastal deltas in the future.

1. Introduction

Coastal wetlands provide many ecosystem services that benefit society, such as storm protection, nutrient removal, and habitat value. They are among the most productive environments on earth with low soil oxygen conditions that facilitate a significant amount of organic matter accumulation and carbon storage (DeLaune and White 2012). Between 1932 and 2016, coastal Louisiana lost 4,833 km^2, or ~25%, of its 1932 land area (Couvillion et al. 2017). While wetland loss rates have decreased since a peak in the 1970s, a majority of Louisiana's coastal basins still experience negative rates of land area change each year (Couvillion et al. 2017). Historically there were avulsions of the Mississippi River flooding large areas of coastal deltaic floodplains, expanding emergent wetlands in coastal hydrologic basins as part of the active phase of the delta cycle. The extensive system of federal levees and river control structures along the Mississippi River constructed as part of the Mississippi & Tributaries Act of 1928 have disconnected wetlands from riverine sediment and nutrients in several coastal basins (Twilley et al. 2016). Terrebonne Bay is a hydrologic coastal basin that has been disconnected from river sediments, forming an inactive delta basin that experiences high rates of wetland loss and Gulf of Mexico landward migration as more marshes are convereted to open-water areas (Twilley et al. 2016; Couvillion et al. 2017). In contrast, the Atchafalaya Bay gets 30% of the combined flow of Mississippi and Red River managed by the Old River Control Structure providing sediment through the Atchafalaya River, forming the Wax Lake and Atchafalaya Deltas, and into the Atchafalaya and Fourleague Bays. Fourleague Bay is a microtidal system that has strong connectivity between river discharge and wind direction and the contribution of riverine sediment and bed resuspension to adjacent wetlands (Perez et al. 2000; Wang et al. 2018; Restreppo et al. 2019). The Atchfalaya and Wax Lake Deltas are active coastal deltaic

floodplains that continue to increase land area since 1974 (Fitzgerald 1998; Wellner et al. 2005), and adjacent wetlands to the Atchafalaya Bay and Fourleague bay have maintained their land area compared to other inactive coastal basins in coastal Louisiana (Twilley et al. 2016).

Coastal basins of the Mississippi River Delta have extremely high rates of relative sea level rise (RSLR) that contribute to vulnerability of coastal wetlands in future scenarios of climate change. Understanding the factors that contribute to adaptations of wetland productivity is very important in predicting how coastal wetlands and the social benefits they provide can reduce vulnerability to future climate change. One key factor determining the ecological adaptation and survival of coastal delta wetlands is marsh platform elevation, which is the surface elevation of the floodplain in relation to a tidal datum. Wetland platform elevation defines the hydroperiod such as flooding frequency and duration, which controls rates of allochthonous sediment deposition, nutrient exchange, and soil stressor formation (Morris et al. 2002; Day et al. 2011; Twilley et al. 2019). Platform elevation of coastal deltaic floodplains can be characterized into separate hydrogeomorphic (HGM) zones (supra-, inter-, and subtidal) that are host to distinct vegetation communities that experience different tidal regimes due to their elevation (Steiger et al. 2005; Bevington and Twilley 2018; Christensen et al. 2020). Net surface elevation change of wetland platforms is the net result of coupled processes of surface sediment (inorganic and organic) deposition, above ground vegetation dynamics, belowground production, soil compaction, decomposition, and subsidence (Allen 2000; Morris 2006; Fagherazzi et al. 2012). These processes occur at different depths in the soil column of wetland platforms representing rates of surface accretion, shallow subsidence, and deep subsidence (Cahoon et al. 1995).

There are three techniques used to measure the rate of soil formation in marsh platforms based on vertical accretion and shallow subsidence. Long-term vertical accretion rates (20-60 years), which measure vertical accretion and shallow subsidence, can be measured using ^{137}Cs core dating techniques, which has been successfully used throughout coastal Louisiana's wetlands (Delaune et al. 1978; Delaune et al. 1983; Nyman et al. 1990; Neubauer et al. 2002; Nolte et al. 2013; Breithaupt et al. 2018). Cesium-137 (^{137}Cs) is a radioisotope that was deposited on earth's surface as a product of thermonuclear weapons testing in the 1950-1970s with peak quantities detected in 1963 (Pennington et al. 1973). Lead-210 (^{210}Pb) is a naturally occurring radioisotope that can also be used to estimate soil age utilizing the constant initial concentration model and works on a longer timescale (5-150 years) than ^{137}Cs dating (Pennington et al. 1976; Appleby and Oldfield 1978; Breithaupt et al. 2018; Baustian et al. 2021). A much shorter time scale of surface accretion, and thus processes contributing to soil formation, is measured using feldspar marker horizons over the course of a few years (Knaus and Cahoon 1990; Cahoon et al. 1996). This method is commonly used to compare surface inputs to soil formation that are useful in monitoring changes in sediment delivery, such as in Louisiana's CRMS (Coastal Reference Monitoring System) field sites that are maintained by Louisiana's Coastal Protection and Restoration Authority's (CPRA) (Folse et al. 2018).

The relative contribution of surface (annual accretion) and subsurface (belowground biomass) processes to soil development were measured to understand the adaptation of wetland platform elevation to RSLR in the presence and absence of river input. Study sites were established in a coastal basin that represents an active delta with riverine sediment input, the Atchafalaya Bay, and in a coastal basin that represents an inactive delta, Terrebonne Bay, where riverine input has been discontinued since 1904. Within each of these experimental coastal

basins, sites were located along a salinity gradient from fresh to saline at the basin level and along local gradients in either HGM zones or distance interior from tidal creeks.

This study investigates the following research questions: (1) What is the influence of coastal basin delta cycle, salinity, and localized site effects (HGM zone and zonation from shore) on short-term vertical accretion rates? (2) What is the influence of coastal basin delta cycle, salinity, and localized site effects (HGM zone and zonation from shore) on inorganic and organic sedimentation rates? (3) How does the inclusion of belowground necromass along with biomass as part of subsurface processes contribute to soil formation across active vs. inactive delta basins and local factors such as salinity and localized site effects (HGM zone and zonation from shore)? I expected sedimentation rates to be lower in Terrebonne Bay sites as this area is a part of the abandoned, inactive delta cycle of the Mississippi River and there is no riverine input of sediment (Hudson 2005; Twilley et al. 2016). In contrast, the Atchafalaya Bay is part of the active delta cycle with high riverine sediment input. The selected brackish and saline sites in the active basin are adjacent to Fourleague Bay, which recieves distal sedimentation from the Atchfalaya River and Wax Lake Deltas, so I also presumed that sedimentation rates along the Atchafalaya Bay salinity transect (fresh to brackish to saline) would decrease with increased distance from the sediment source (Twilley et al. 2019). Along HGM gradients, I assumed that inorganic sedimentation rates would decrease with increased elevation as supratidal elevations experience less tidal inundation (Törnqvist et al. 2021). I also expected that belowground biomass and necromass dynamics would be significant to long-term accretion rates, and stocks of BGB would be similar among sites within the same salinity zone and not necessarily the same coastal basin.

A major limitation of using the feldspar marker horizon method compared to vertical accretion rates measured by ^{137}Cs and ^{210}Pb is that marker horizons only capture a short-term (months to a few years) surface accretion signal that is highly variable. Marker horizons are also not able to capture effects of longer decadal-scale soil processes such as shallow subsidence (associated with soil compaction) and organic matter decomposition (Breithaupt et al. 2018). Soil cohort models can be used to integrate the relative significance of these processes that occur at different time scales to understand what controls soil formation and thus wetland platform elevations. I modified a soil cohort model to investigate the relative significance of surface accretion rates from feldspar marker horizons in active and inactive delta basins to understand how they contribute, along with belowground processes, to longer term sediment accretion rates (^{137}Cs and ^{210}Pb) and adaptation of delta floodplain surface elevations. I wanted to answer, based on model simulations, how do contributions of surface and subsurface processes vary in soil development and marsh platform accretion over decadal time scales in active vs. inactive delta basins; and are there gradients across salinity and HGM zones within each basin type?

One of the first models created to simulate inorganic and organic matter accumulation in marsh soils was the SEMIDEC model (Morris and Bowden 1986), and several cohort models have been adapted from SEMIDEC, including the nutrient mangrove (NUMAN) model (Chen and Twilley 1999) and Relative Elevation Model (REM) (Rybczyk et al. 1998). This study adapts the NUMAN model to marshes (NUMAR, numerical marsh accretion and response) and aims to apply characteristics of newly accreted soil material, model soil organic matter development, and estimate long-term sediment accretion rates (70 years). Like SEMIDEC and its other descendants, the NUMAR model utilizes one-year soil cohorts, separates material within inorganic, refractory organic, and labile organic matter pools, and accounts for belowground

biomass production using an exponential decay root distribution with depth. The NUMAR model provides an opportunity to use surface accretion rates from feldspar marker horizons (surface sedimentation) combined with belowground biomass production and decompositon rates (subsurface processes) to estimate decadal accretion in coastal wetlands. These decadal sediment accretion rates are of interest to coastal engineers working in coastal wetland restoration and matainence, because sediment accretion builds elevation capital and is a key determinent of surface elevation change rates. Rates of change in wetland surface elevation inform engineers on a wetland's resiliency to RSLR and whether a coastal wetland can keep pace with RSLR (high integrity) or will decrease elevation capital and become submerged (low integrity) (Cahoon et al. 2019).

Comparing rates of surface and subsurface processes that contribute inorganic and organic sedimentation to soil development in active and inactive delta basins along salinity and HGM gradients provide insights to how engineering projects can enhance marsh creation using sediment input scenarios. The delta mass balance model (Paola et al. 2011) describes how surface sedimentation and subsurface root production contribute to delta formation. The field experiments and modeling exercises described in this thesis test the relative contribution of each to filling the accomodation space of coastal deltas with different degrees of river connectivity.

2. Methods

2.1. Study Sites

Study sites were selected along salinity gradient (freshwater, brackish, and saline) within the Atchafalaya Bay (active delta basin) and Terrebonne Bay (inactive delta basin) as engineered hydrologic basins of the Mississippi River Delta Plain (Figure 1). Marsh types were determined on the basis of species composition and abundance from a U.S. Geological Survey report (Sasser et al. 2014). Fourleague Bay marsh sites in this study were included in the Atchafalaya Bay as Fourleague Bay is connected to the Atchafalaya River discharge, which delivers suspended sediment and nutrients to the adjacent bay and marshes (Madden et al. 1988; Perez et al. 2000; Lane et al. 2011). The Atchafalaya Bay freshwater site located on Mike Island of Wax Lake Delta (WLD) is an active coastal deltaic floodplain, which had supratidal HGM zones dominated by *Colocasia esculenta* and *Salix nigra*, intertidal zones by *Nelumbo lutea*, and subtidal zones by submerged aquatic vegetation (SAV) (Bevington and Twilley 2018; Jensen et al. 2021). The freshwater site (CRMS 0294) in the inactive Terrebonne Bay was a floating marsh dominated by *Polygonum punctatum*, *Eleocharis montana*, and *Typha domingensis* (CPRA 2022). Brackish sites in active Atchafalaya Bay (CRMS 0399) and inactive Terrebonne Bay (CRMS 0396) were both dominated by *Spartina patens.* Saline sites in Atchafalaya Bay (CRMS 0322) and Terrebonne Bay (CRMS 0421) were either dominated by *Spartina patens* or *Spartina alterniflora*. Five of the six study sites were intertidal marshes located at Coastwide Reference Monitoring Systems (CRMS) stations.

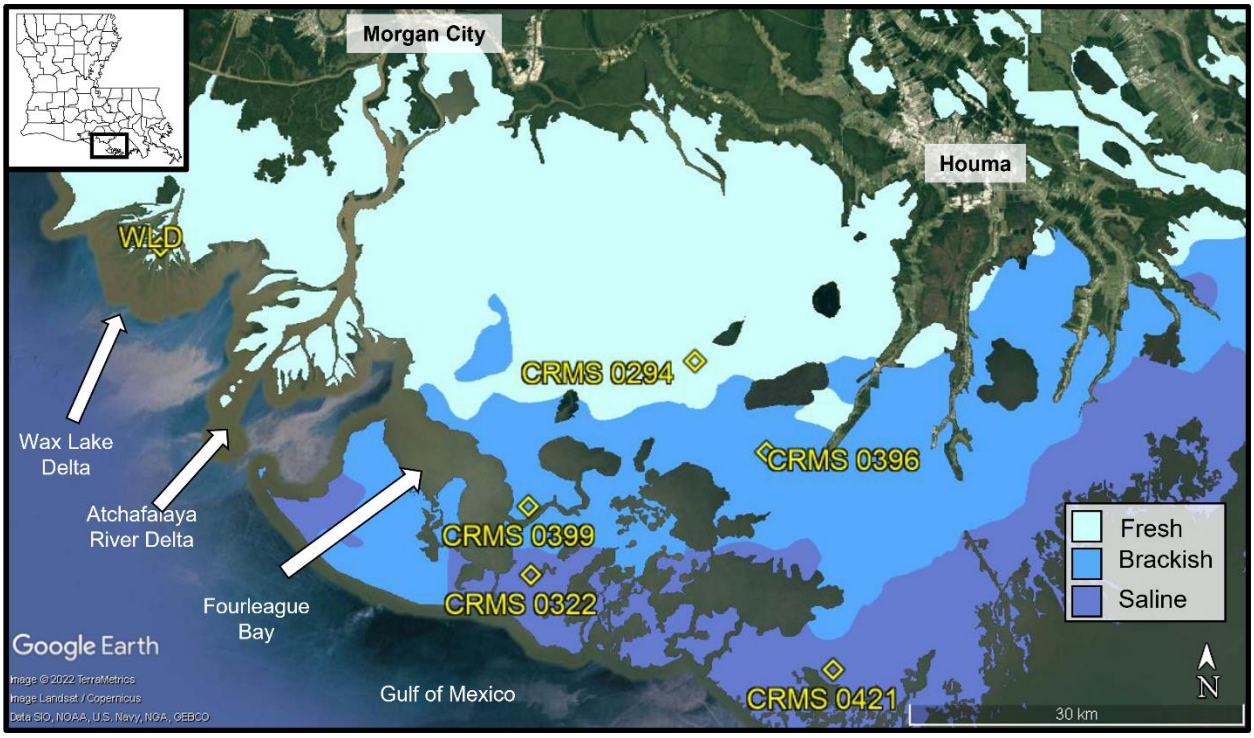

Figure 1. Site locations in southeast Louisiana near Morgan City and Houma, LA. Marsh type zones (fresh, brackish, and saline) from coastwide reference monitoring stations (CRMS) vegetation surveys are shown in shades of blue. The intermediate marsh type was combined with brackish marshes. Marsh type GIS layers downloaded from the Coastal Information Management System (CIMS) database of Louisiana's Coastal Protection and Restoration Authority (CPRA). Inset map image from USGS of Louisiana Parishes.

2.2. Surface Accretion Measurements

Feldspar stations were deployed with triplicate feldspar marker horizon plots in Fall 2019 and sampled at 12, 18, and 24 months using a cryo-coring technique with liquid nitrogen (Cahoon et al. 1996; Folse et al. 2018). Feldspar stations were accessed by airboat and a removable boardwalk and table setup to minimize disturbance of plots during sampling (Figure 2). Two cryo-cores were taken from two non-repeating, randomized plot locations in each of the triplicate feldspar plots at each sampling interval (Figure 3). Each cryo-core was measured three times with calipers to the nearest millimeter, and measurements were averaged to a singular accretion measurement per cryo-core. A total of sixteen feldspar stations were deployed and sampled as previously described: two intertidal feldspar stations at each of the five CRMS study

sites and six feldspar stations at WLD (Figure 4). Three feldspar stations (supra-, inter-, and subtidal) were deployed along two transects in different chronosequence zones (I and III) (Aarons 2019) of Mike Island in WLD (Figure 5).

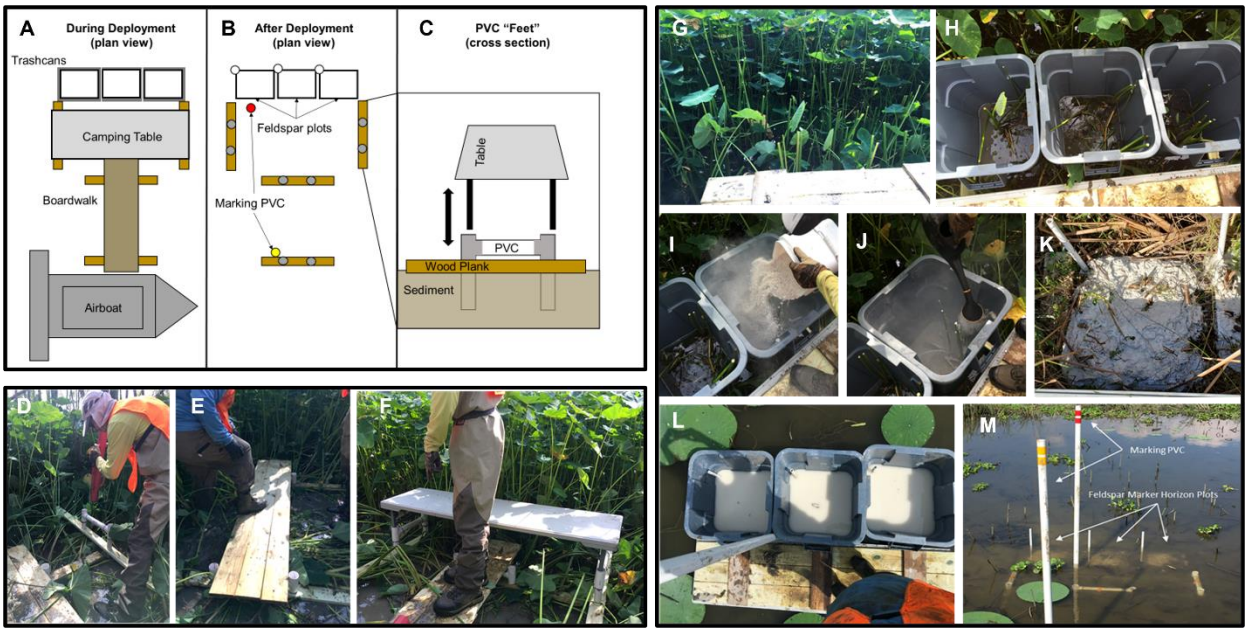

Figure 2. Schematic of feldspar station design during (A) and after deployment (B) with cross-section of PVC feet supports (C). Images during installation of PVC feet (D) to hold removable boardwalk (E) and table (F). Steps to deploy feldspar marker horizon including clipping vegetation (G), placing trashcans (H), sprinkling feldspar into trashcans (I), wetting marker horizon if no water present (J) to produce a caking effect (K) or waiting 20 minutes if standing water is present for feldspar to settle (L). After deployment, boardwalk and table were removed (M).

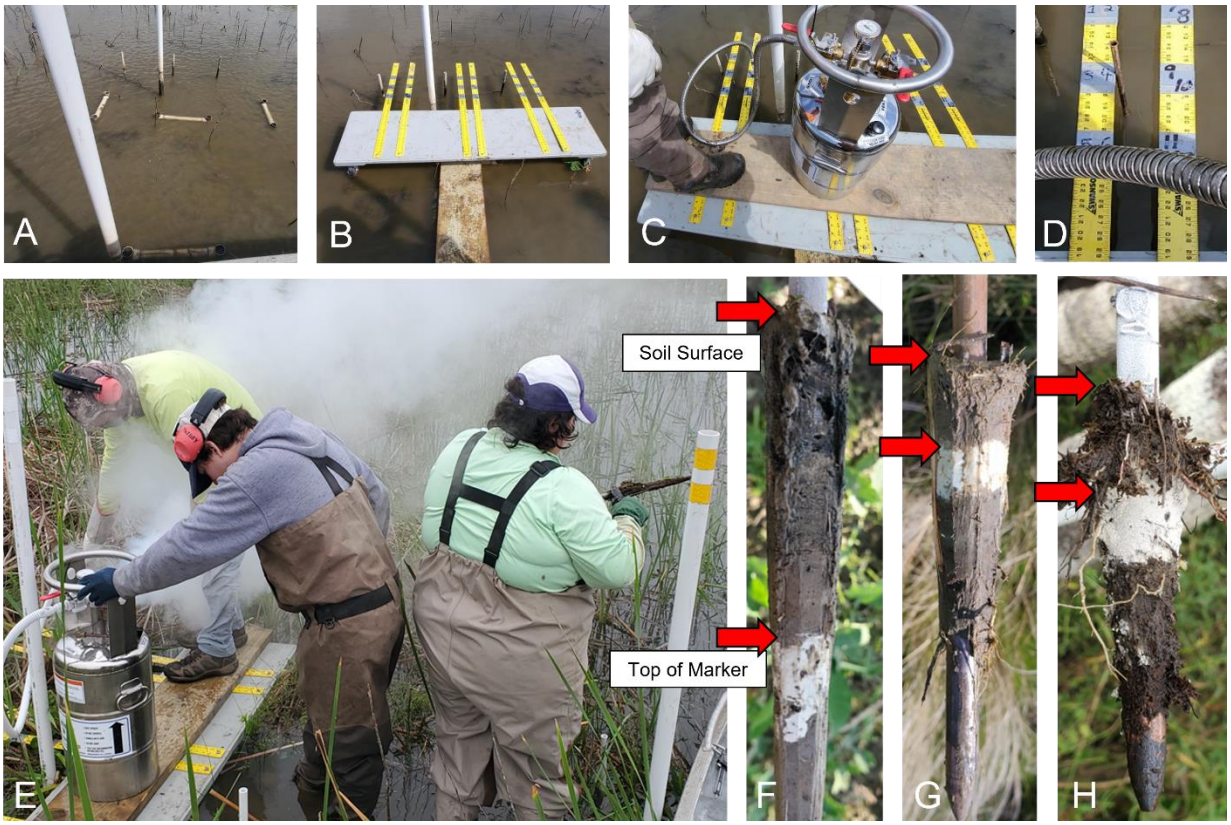

Figure 3. After arriving to each Feldspar Station (A) the table and boardwalk is placed (B). Cryo-cores are collected using a liquid nitrogen dewar, hose, and copper “bullets” (C). The outer sheath of the copper bullet is placed in the soil at a non-repeating random location in the marker horizon (D). Liquid nitrogen is pumped into the bullet sheath until a thin layer of soil is frozen around the bullet and the bullet can be removed from the ground (E). The resulting frozen soil is cleaned off with a knife, and the distance between the soil surface and the top of the feldspar marker horizon (surface accretion) is measured three separate times with calipers. Examples of collected cryo-cores are in panels F, G, and H.

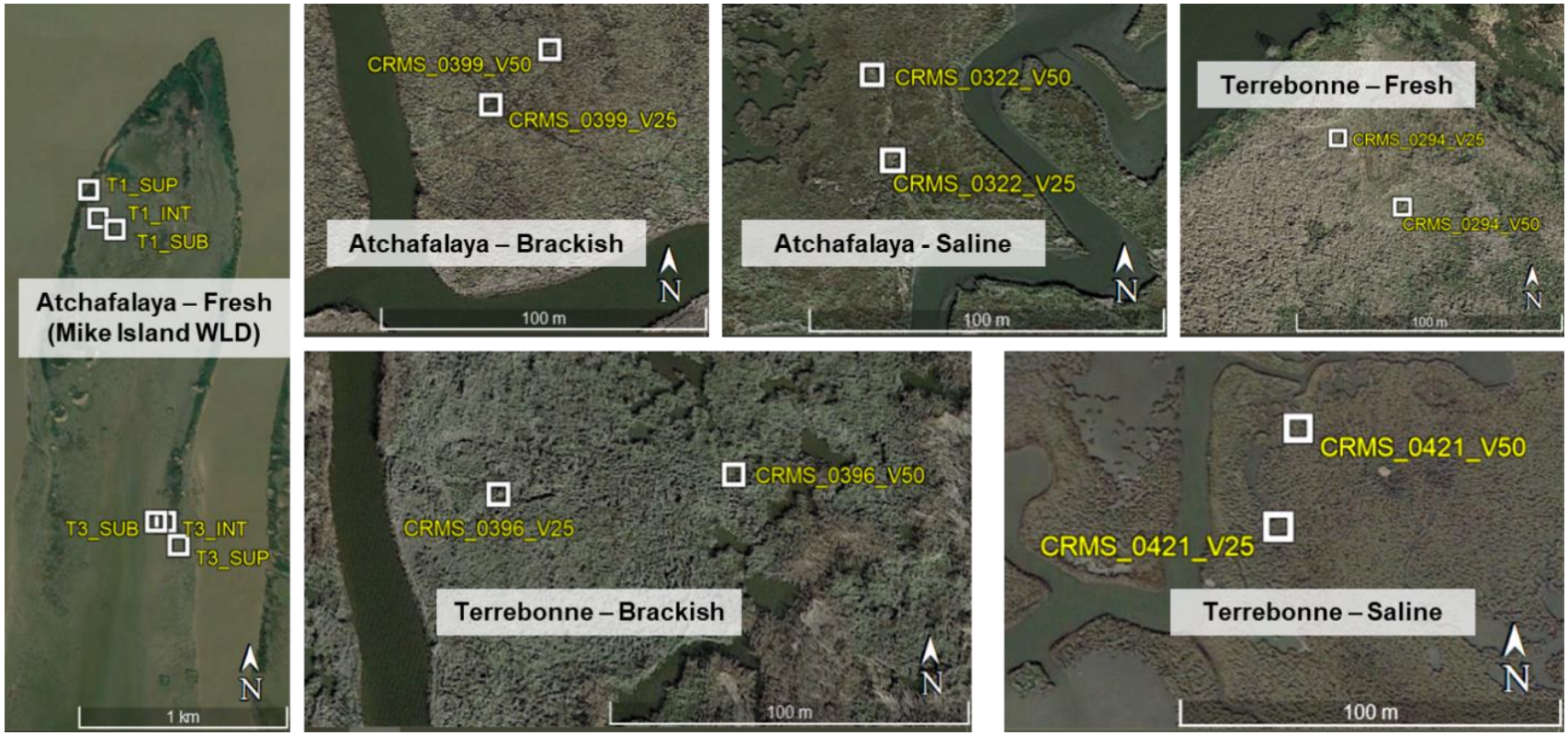

Figure 4. Feldspar stations at each study site. Coastwide reference monitoring station (CRMS) sites had two intertidal feldspar stations ~25m and ~50m inland from a tidal channel. At Mike Island in Wax Lake Delta (WLD), two transects were established at older (northern) and younger (southern) areas with three feldspar stations at three hydrogeomorphic (HGM) of supratidal, intertidal, and subtidal locations.

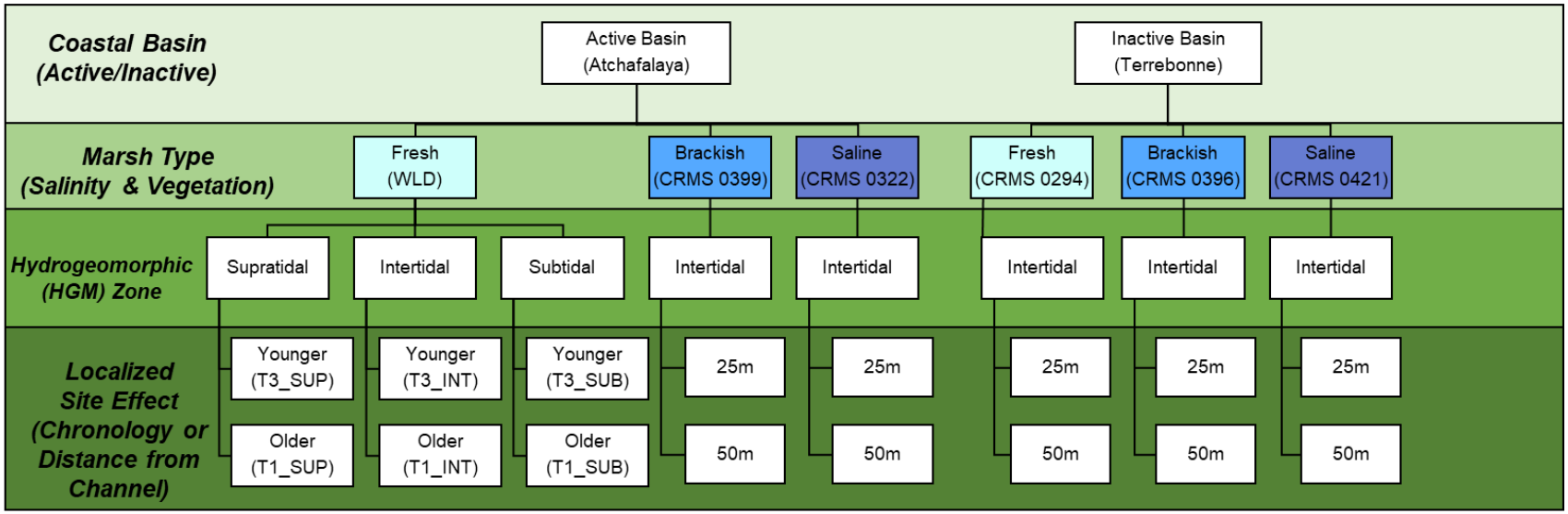

Figure 5. Sampling design hierarchy of feldspar stations with coastal basin – marsh type – hydrogeomorphic (HGM) zone – and localized site effects.

2.3. Soil Physicochemical Characteristics

For each cryo-core collected, a soil core was collected near the corresponding feldspar station and sectioned to the depth corresponding to the average surface accretion measurement for that unique cryo-core. Samples were temporarily stored in Whirlpaks at 4°C in the laboratory until they could be oven-dried at 60°C to a constant weight. Bulk density of samples was determined by dividing the dry weight of the soil sample by its wet volume. Soil samples were ground using a Wiley Mill and passed through a 250-μm-mesh.

For each sample, two analytical replicates were combusted in a muffle furnace at 550°C for 2 hours, and the organic matter (OM) concentration (% dry mass) of each sample was determined by the mass that was lost on ignition (LOI) (Davies 1974). For each sample, two analytical replicated were weighed into silver capsules and fumigated in a desiccator with 12M hydrochloric acid to remove inorganic carbonates before capsules were combusted in a ECS 4010 elemental analyzer (Costech Analytical Technologies, Inc., Valencia, CA) for total organic carbon (TOC) (Harris et al. 2001). Organic matter and organic carbon were expressed on a volume basis using sample bulk density (g cm^{-3}). Composite soil samples from each CRMS site and feldspar station in WLD were analyzed for the percent acid detergent lignin of organic matter (ADL % OM) at the LSU AgCenter Forage Testing Lab (Van Soest 1963), and average OM (% dry mass) of composite sample groups were used to estimate the lignin fraction (g g^{-1}) of soil samples to be used in the NUMAR model.

2.4 Belowground Biomass and Decomposition

During peak biomass in Fall 2020, four belowground biomass (BGB) cores (10cm diameter) were collected at each CRMS site. At WLD, nine BGB cores were collected at both supratidal and intertidal locations. All BGB cores were sectioned by depth into 0-10, 10-20, 20-

30, 30-40, and 40-50cm sections. Core sections were rinsed on a 500μm mesh sieve, and the mass remaining on top of the mesh was separated and categorized as either biomass or necromass using a combination of buoyancy testing (biomass floats and necromass sinks) and visual assessment (biomass is lighter in color with higher turgidity) (Giraldo Sánchez 2005; Castañeda 2010). Biomass and necromass samples were then oven-dried to a constant weight at 30°C, and the biomass and necromass of each core section was calculated as the dry biomass or necromass divided by the core area (78.5cm^2) for each 10cm section.

The depth integrated mass (R_I) for each core was the sum of the five 10cm sections with either biomass only or total root mass (biomass and necromass combined). In cases when only a 40cm deep core could be collected, the sum of those four 10cm sections was multiplied by 1.25 to normalize that core to a 50cm depth. Belowground mass values were averaged between cores at the same site, and WLD cores were analyzed separately by HGM zone (supratidal and intertidal). For each site, composite BGB and composite belowground necromass samples were analyzed in triplicate for ash fraction (fc1) using loss on ignition (Davies 1974) and for refractory fraction (fc0) using acid detergent lignin analysis (Van Soest 1963).

Collected BGB core material was also used in an in-situ decomposition experiment along with senesced above ground biomass (AGB). Decomposition bags were prepared in 1mm-mesh aquarium filter bags (15 x 20 cm) with aluminum tags, filled with a known weight of material from the site they were deployed at, and attached to PVC poles with fishing line (Brinson et al. 1981; Twilley et al. 1985; Cormier et al. 2015). For each site, four PVC poles were deployed, each with a set of 12 decomposition bags attached: three of senescing AGB (soil surface), three senescing AGB (buried), three BGB (buried), and three belowground necromass bags (buried)

(Figure 6). Decomposition stations were deployed at both an intertidal and a supratidal location at WLD.

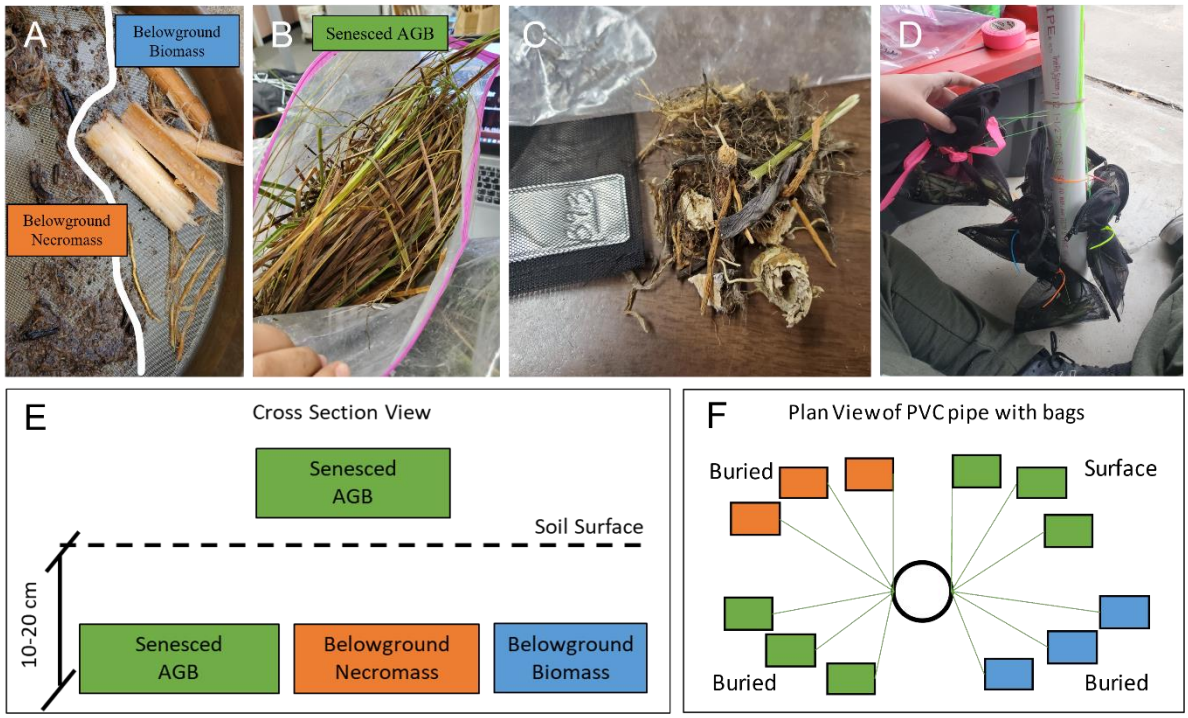

Figure 6. Examples of collected belowground biomass and necromass (A) and senesced aboveground biomass (B). Material was dried and put into aquarium mesh bags with an aluminum tag (C) and attached to a 10-foot PVC pole using fishing line (D). Each PVC pole had a set of 12 bags: 3 buried above ground biomass (AGB), 3 AGB at surface, 3 belowground biomass (BGB), and 3 belowground necromass buried, shown as a cross section (E) and plan view (F).

After six months in the field, two of the four sets of bags were randomly chosen to be collected at each site (Summer 2021), and the remaining two sets were collected at 12 months (Winter 2021). After collection, decomposition bags were stored at 4°C until they could be rinsed and oven-dried at 30°C until constant weight. The yearly decomposition rate (yr^{-1}) for each site was calculated using a single exponential decay model (*1*):

$$M_t = M_0 e^{-kt} \rightarrow k = \frac{\ln\left(\frac{M_t}{M_0}\right)}{-t} \quad (1)$$

where M_t is the mass remaining after time (t), M_0 is the beginning mass, and k is the decomposition rate (Brinson et al. 1981; Bärlocher 2005). For each site, the natural log of the percentage of mass remaining was linearly regressed with time in years in R to calculate the decomposition rate k (Bärlocher 2005; Stagg et al. 2018; Middleton 2020) (*2*).

$$\ln(M_t) = \ln(M_0 * e^{-kt}) \rightarrow \ln(M_t) = \ln(M_0) * -kt \rightarrow \ln\left(\frac{M_t}{M_0}\right) = -kt \quad (2)$$

3. Results

3.1. Surface Accretion Rates and Physicochemical Characteristics

ANOVAs were performed between linear models that either did or did not include a localized site level interaction term (either distance from channel or chronology). There were no significant differences (p-value > 0.05) between surface accretion rates measured at 25m and 50m inland feldspar stations at CRMS study sites except for the active brackish marsh site (CRMS 0399). Surface accretion data from the 25m and 50m inland feldspar stations at the same site were combined to calculate surface accretion rates at the HGM zone level (Table 1). In WLD, where island chronology was tested, there was a significant difference between the older supratidal (4.31 cm yr^{-1}) and younger supratidal (7.06 cm yr^{-1}) sites as well as between the older subtidal (4.43 cm yr^{-1}) and younger subtidal (2.62 cm yr^{-1}) sites ($p<0.05$). Surface accretion rates in the older chronology transect were not significantly different among HGM zones ($p = 0.064$), however accretion rates in the younger transect were significantly different between HGM zones ($p<0.05$). Ignoring HGM zones, the surface accretion rate was 4.35 cm yr^{-1} for the older transect ($p<0.001$, df = 56, adjusted $R^2 = 0.93$) and 4.22 cm yr^{-1} for the younger transect ($p<0.001$, df = 41, adjusted $R^2 = 0.73$). Surface accretion data from T1 (older) and T3 (younger) was combined to calculate surface accretion rates at the HGM zone level for WLD (Table *1*). Unfortunately, in WLD, the feldspar markers at the younger (T3) intertidal station were lost after 12 months from erosion and are not included in these results.

Table 1. Surface accretion rates from feldspar marker horizons at study sites. Rates ± standard error and adjusted R^2 values were calculated using a linear regression model in R. All rates shown were calculated using data from two feldspar stations over three sampling periods (12, 18, and 24 months) except for the singular surviving intertidal Wax Lake Delta (WLD) feldspar station. Asterisks (*) denote rates that are statistically significant (p-value <0.05).

Basin	Salinity	HGM zone	Site	Surface Accretion Rate ± SE (cm yr^{-1})	P-value	Adjusted R^2 Value	Degrees of Freedom
Atchafalaya	Fresh	Supratidal	WLD	5.74 ± 0.37*	< 0.001	0.85	40
Atchafalaya	Fresh	Intertidal	WLD	4.32 ± 0.38*	< 0.001	0.88	17
Atchafalaya	Fresh	Subtidal	WLD	3.51 ± 0.22*	< 0.001	0.86	29
Atchafalaya	Brackish	Intertidal	CRMS 0399	1.42 ± 0.12*	< 0.001	0.80	35
Atchafalaya	Saline	Intertidal	CRMS 0322	1.42 ± 0.09*	< 0.001	0.88	35
Terrebonne	Fresh	Intertidal	CRMS 0294	2.03 ± 0.14*	< 0.001	0.84	39
Terrebonne	Brackish	Intertidal	CRMS 0396	2.27 ± 0.23*	< 0.001	0.71	36
Terrebonne	Saline	Intertidal	CRMS 0421	3.14 ± 0.23*	< 0.001	0.84	33

For each combination of two sites (28 total combinations), a pair of linear models were fit with and without a site interaction term. ANOVAs were used for each pair of linear models to test for significant differences between sites. Surface accretion rates of every site were significantly different ($p<0.05$) from one another except for the active brackish and saline sites (CRMS 0322 vs. 0399) and the inactive fresh and brackish sites (CRMS 0294 vs. 0396). Sites were grouped by hand using results from the 28 ANOVA tests (Figure 7).

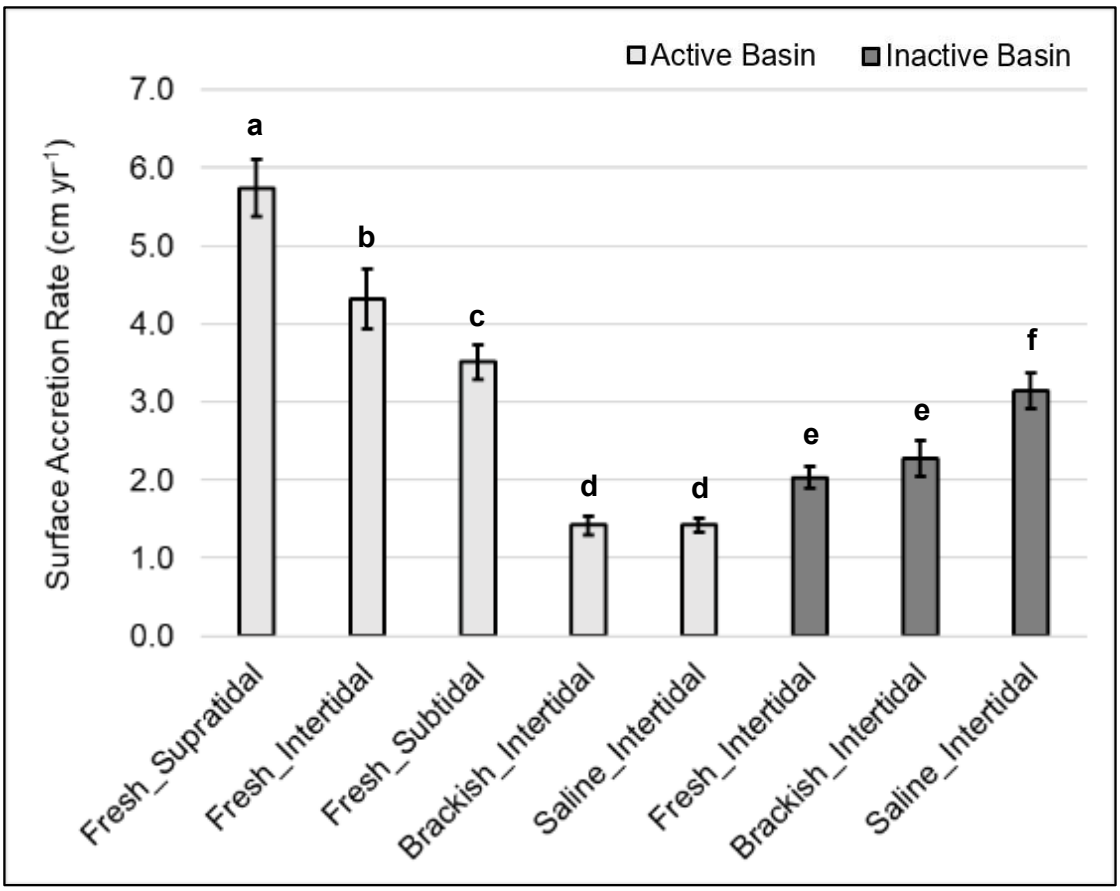

Figure 7. Surface accretion rates from feldspar marker horizons at study sites. Average accretion rates ± standard error were calculated using a linear regression model of accretion data from three sampling periods (12, 18, and 24 months). Lowercase letters above each bar denote statistically significant groups. If two bars have different letters above them, surface accretion rates for those sites are significantly different from each other ($p<0.05$).

Collected soil samples of depths corresponding to each sampled cryo-core were assumed to represent surface accreted material at each site. Physicochemical characteristics of bulk density, organic matter (% dry mass), organic matter density (g cm^{-3}) and organic carbon density (g cm^{-3}) of the surface accreted material were compared at the site HGM zone level using ANOVA and Tukey post-hoc testing (Figure 8). Bulk densities were significantly higher at the Atchafalaya fresh (WLD) sites than the other marshes (Figure 8A), and the opposite trend was found with organic matter (% dry mass) with the highest concentrations found in the fresh and brackish inactive basin sites (Figure 8B). Organic matter densities for the fresh supratidal,

brackish, and saline sites in the active basin were significantly higher than in the inactive basin ($p<0.05$) (Figure 8C). Organic carbon densities of the active brackish and saline marshes in Fourleague Bay were significantly higher than all other sites ($p<0.05$) (Figure 8D).

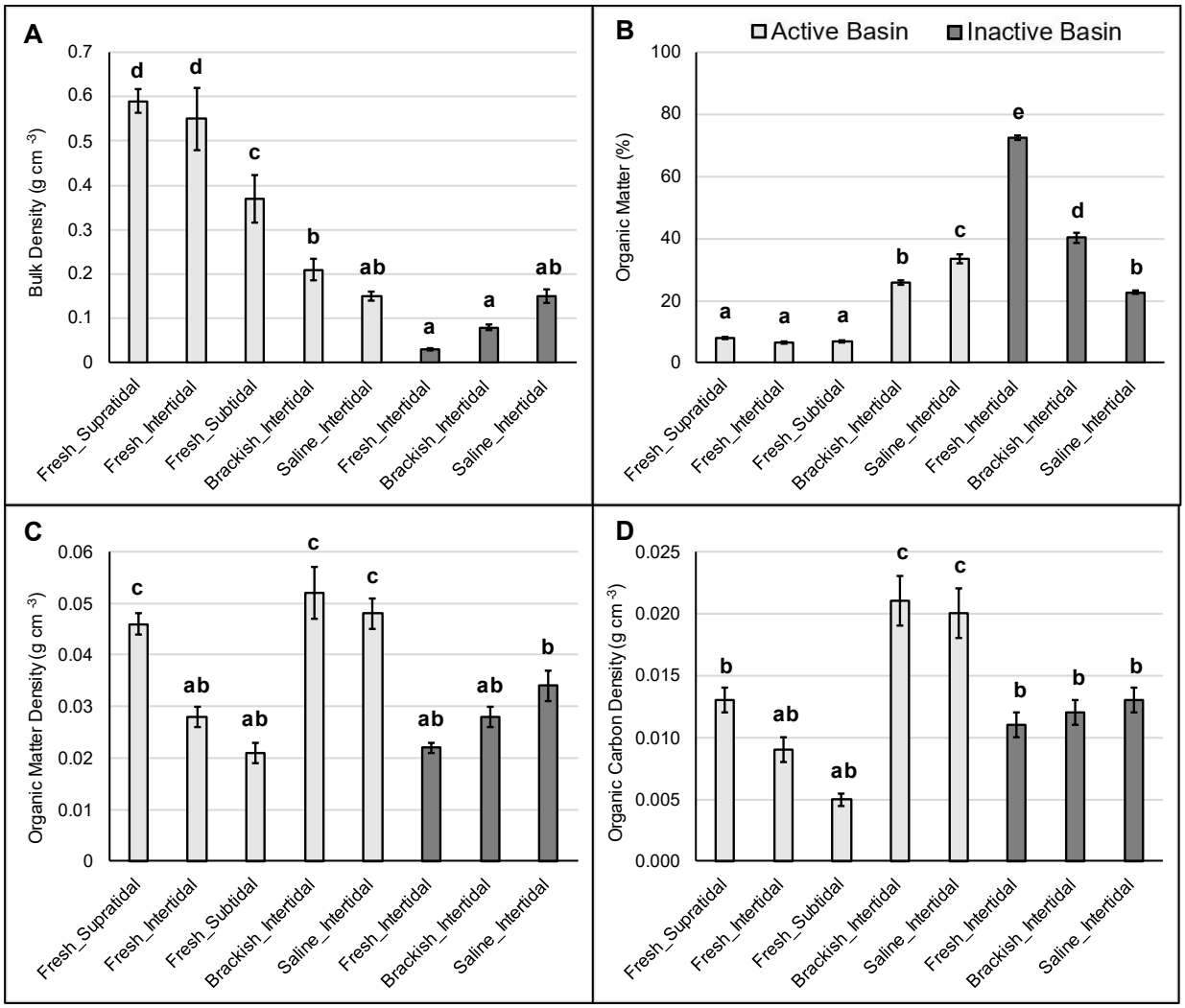

Figure 8. Average ± standard error of surface accreted bulk density (A), organic matter concentration (% dry mass) (B), organic matter density (C), and organic carbon density (D). Organic matter density (g cm^{-3}) is the product of bulk density (g cm^{-3}) and organic matter concentration. Organic carbon density (g cm^{-3}) is the product of bulk density and total organic carbon (TOC) concentration. Compact letter display (cld) above each bar display groups assigned as the results from post-hoc Tukey testing done in R. If a bar has any of the same letters as another bar in the same panel, those two sampling groups are not significantly different from each other (p-value > 0.05).

The lignin fraction of composite sediment samples varied by site in a similar pattern as organic matter concentration. The mineral sediment of active fresh sites at WLD was only ~8% organic matter by dry mass with ~2% of that organic matter being ADL, yielding lignin fractions of <1% of the sediment dry mass. In contrast, soil in the inactive fresh site was >70% organic matter with ~45% of that organic matter being ADL by mass (lignin fraction of ~30% sediment dry mass). The remaining sites had lignin fractions ranging from 2% to 7% of sediment dry mass.

3.2 Inorganic and Organic Sedimentation Rates

The inorganic, organic matter, and organic carbon sedimentation rates (g cm^{-2} yr^{-1}) for each site were calculated by multiplying the mean feldspar surface accretion rate (cm yr^{-1}), surface accreted soil bulk densities (g cm^{-3}), and inorganic, organic matter, and total organic carbon concentrations (g g^{-1}) of surface accreted soil samples. Inorganic sedimentation rates in WLD, an active coastal deltaic floodplain, was higher than all other sites, and rates decreased along the HGM zone gradient (supratidal to intertidal to subtidal) (Figure 9A). Active brackish and saline sites had significantly lower ($p < 0.05$) inorganic sedimentation rates than the active fresh site at WLD. In the inactive basin, mean inorganic sedimentation rates increased with salinity from fresh (0.017 ± 0.001 g cm^{-2} yr^{-1}) to brackish (0.108 ± 0.012 g cm^{-2} yr^{-1}) to saline (0.381 ± 0.041 g cm^{-2} yr^{-1}) (mean ± standard error). Organic matter and organic carbon accumulation rates in the inactive basin also increased with increasing salinity, with the saline site having significantly higher rates than fresh and brackish sites in both cases (Figure 9B, Figure 9C). Fresh subtidal, brackish, and saline sites in the active basin had similar rates of organic matter and organic carbon accumulation, and organic accumulation rates decreased along the HGM zone gradient with decreasing elevation in WLD (Figure 9B, Figure 9C).

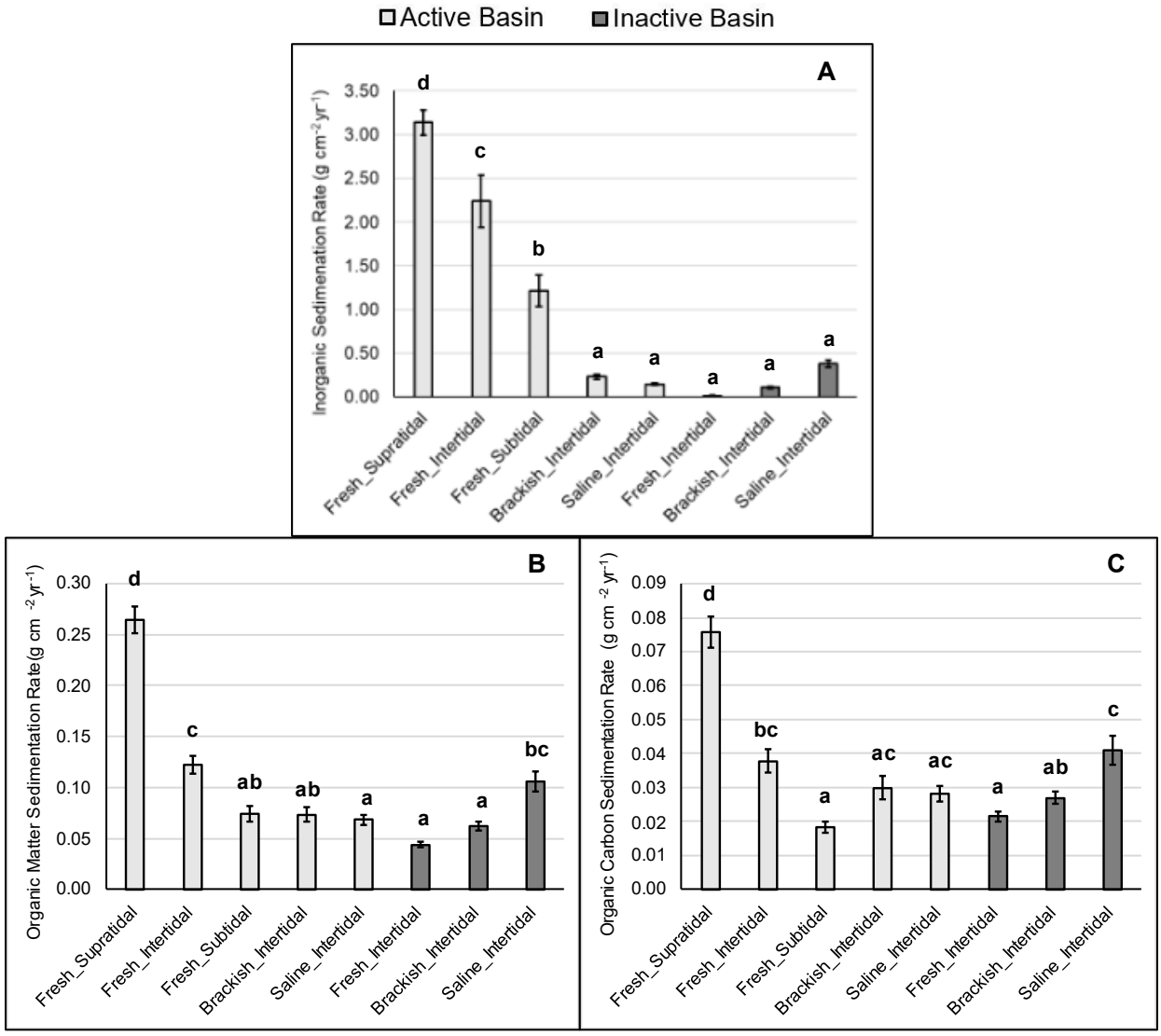

Figure 9. Inorganic (A), organic matter (B), and organic carbon sedimentation rates (C) (g cm^{-2} yr^{-1}) were calculated using average surface accretion rates from feldspar marker horizon stations multiplied by bulk densities and inorganic, organic matter, and total organic carbon concentrations of surface accreted soil samples. Values shown are averages ± standard error, and compact letter display (cld) above each bar display groups assigned as the results from post-hoc Tukey testing done in R. If a bar has any of the same letters as another bar in the same panel, those two sampling groups are not significantly different from each other (p-value > 0.05)

3.3 Belowground Biomass and Decomposition

Belowground biomass and total root mass for 50cm cores were compared at the site and HGM zone level using ANOVA and Tukey post-hoc testing. The addition of belowground necromass to calculate total root mass significantly increased each site's BGB except for the active fresh intertidal site and the inactive saline site ($p<0.05$) (Figure 10). Average belowground biomass ranged from 600-5500 g m^{-2} while average total root mass ranged from 3000-11000 g m^{-2}. Saline sites in both basins had the most BGB and total root mass of all study sites (Figure 10). Both BGB and total root mass increased in the active basin with increased salinity.

The inorganic fraction of belowground biomass and necromass was similar for each site and similar to the 0.10 value used in the NUMAN model (Benner et al. 1990; Chen and Twilley 1999) (Table 2). Freshwater sites had average biomass lignin fractions of 0.15-0.24 while their average necromass lignin fractions ranged from 0.50-0.61. In contrast, the brackish and saline sites had average biomass lignin fractions of 0.41-0.48 and average necromass lignin fractions from 0.54-0.59 (Table 2).

Decompositon rates were calculated from a linearly regression of the natural log of % mass remaining over time, and decomposition rates were significant ($p<0.001$) with adjusted R^2 values ranging from 0.77-0.99 (Table 3). Across all sites, bags filled with belowground necromass had the slowest decomposition rates (0.2-0.3 yr^{-1}) while bags filled with senesced AGB and placed on the soil surface had the highest average rate of decomposition (~1.5 yr^{-1}). The fastest decomposition rates of AGB and BGB were observed at the fresh supratidal station in WLD (Table 3).

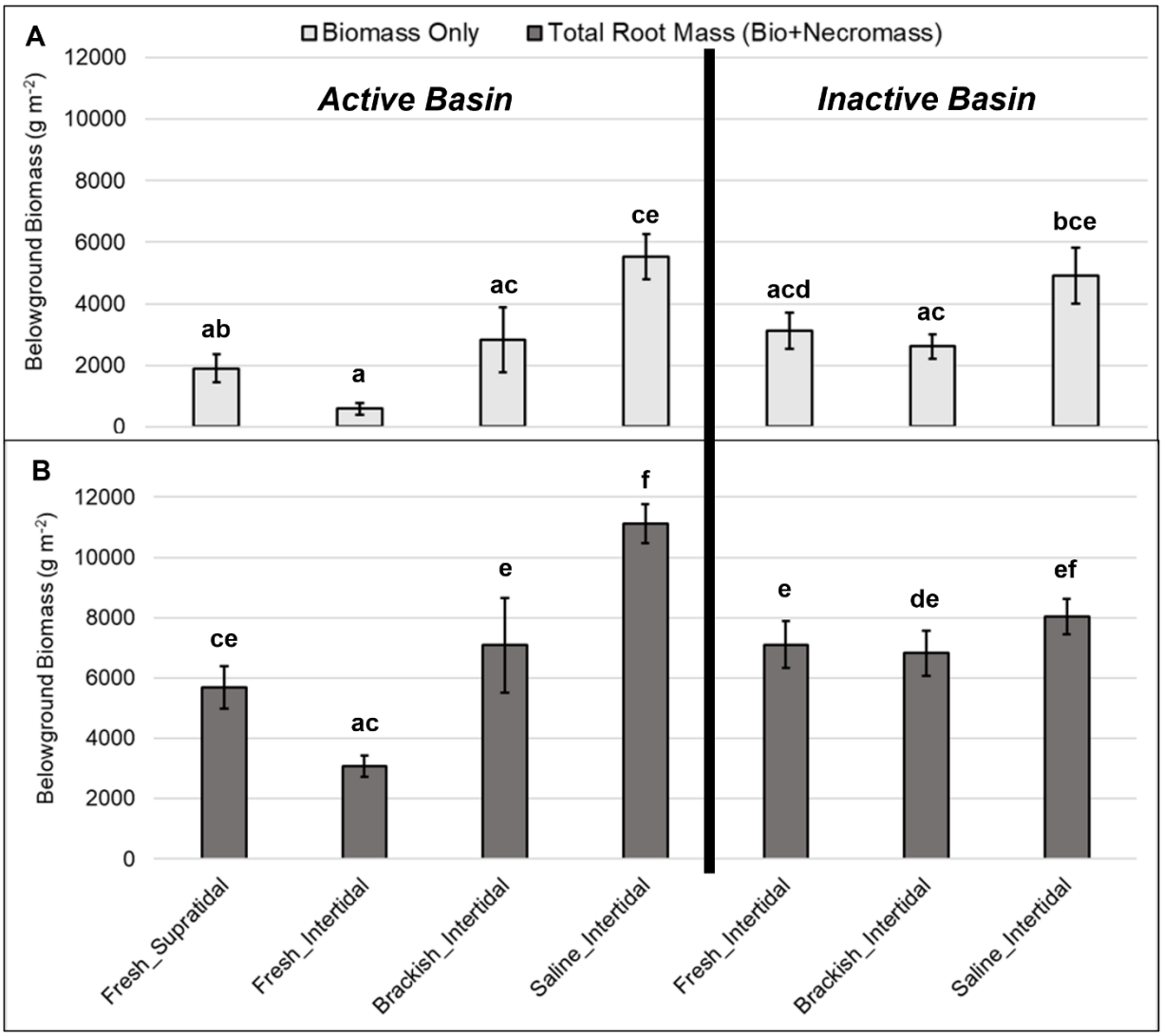

Figure 10. Average ± standard error of belowground biomass (A) and total root mass (bio+necromass) (B) in g m^{-2} for 50cm cores. Compact letter display (cld) above each bar display groups assigned as the results from post-hoc Tukey testing done in R. If a bar has any of the same letters as another bar, those two sampling groups are not significantly different from each other (p-value > 0.05).

Table 2. Mean ± standard error of inorganic and lignin fractions of both biomass and necromass composite samples. The total root mass fractions are weighted means of the biomass and necromass fractions based on the site-specific ratio of biomass:necromass found in collected cores. Inorganic fractions and lignin fractions represent the input parameters fc_1 and fc_0. Degrees of freedom equals 2 for biomass and necromass fractions.

Basin	Salinity	HGM Zone	Site	Biomass Inorganic Fraction (fc1) ($g\ g^{-1}$)	Necromass Inorganic Fraction (fc1) ($g\ g^{-1}$)	Total Root Mass Inorganic Fraction (fc1) ($g\ g^{-1}$)	Biomass Lignin Fraction (fc0) ($g\ g^{-1}$)	Necromass Lignin Fraction (fc0) ($g\ g^{-1}$)	Total Root Mass Lignin Fraction (fc0) ($g\ g^{-1}$)
Atchafalaya	Fresh	Supratidal	WLD	0.07 ± 0.01	0.09 ± 0.02	0.08	0.20 ± 0.06	0.50 ± 0.06	0.40
Atchafalaya	Fresh	Intertidal	WLD	0.09 ± 0.00	0.14 ± 0.04	0.13	0.15 ± 0.06	0.53 ± 0.04	0.46
Atchafalaya	Brackish	Intertidal	CRMS 0399	0.03 ± 0.00	0.03 ± 0.01	0.03	0.41 ± 0.04	0.57 ± 0.02	0.51
Atchafalaya	Saline	Intertidal	CRMS 0322	0.03 ± 0.00	0.05 ± 0.00	0.04	0.43 ± 0.02	0.56 ± 0.00	0.50
Terrebonne	Fresh	Intertidal	CRMS 0294	0.06 ± 0.00	0.05 ± 0.01	0.06	0.24 ± 0.01	0.61 ± 0.03	0.29
Terrebonne	Brackish	Intertidal	CRMS 0396	0.02 ± 0.00	0.03 ± 0.01	0.02	0.48 ± 0.01	0.54 ± 0.03	0.52
Terrebonne	Saline	Intertidal	CRMS 0421	0.04 ± 0.01	0.04 ± 0.01	0.04	0.41 ± 0.011	0.59 ± 0.11	0.48

Table 3. Results of decomposition bag field experiment using collected data from retrieved 6-month and 12-month decomposition bags. Each decomposition rate (k) was calculated using a linear regression model of the natural log of percentage of mass remaining(%Mt/M0) vs. time (t): [ln(%Mt/M0) = e^(-kt)] in R. Asterisks (*) denote decomposition rates that are statistically significant (p-value <0.05). Daggers (†) denote where, unfortunately, no field data is available due to mismanaged bag beginning weight data.

Basin	Salinity	HGM Zone	Site	Decomposition Material	Decomposition Rate (k) (yr^{-1})	P-value	Degrees of Freedom	Adjusted R^2 Value
Atchafalaya	Fresh	Supratidal	WLD	Senesced AGB at Surface	2.46 ± 0.26*	<0.001	11	0.88
Atchafalaya	Fresh	Intertidal	WLD		1.15 ± 0.07*	<0.001	11	0.96
Atchafalaya	Brackish	Intertidal	CRMS 0399		1.23 ± 0.06*	<0.001	11	0.97
Atchafalaya	Saline	Intertidal	CRMS 0322		1.30 ± 0.15*	<0.001	11	0.86
Terrebonne	Fresh	Intertidal	CRMS 0294		1.16 ± 0.10*	<0.001	10	0.93
Terrebonne	Brackish	Intertidal	CRMS 0396		†			
Terrebonne	Saline	Intertidal	CRMS 0421		†			
Atchafalaya	Fresh	Supratidal	WLD	Senesced AGB buried	3.18 ± 0.23*	<0.001	11	0.94
Atchafalaya	Fresh	Intertidal	WLD		0.88 ± 0.04*	<0.001	11	0.98
Atchafalaya	Brackish	Intertidal	CRMS 0399		0.82 ± 0.04*	<0.001	11	0.98
Atchafalaya	Saline	Intertidal	CRMS 0322		0.95 ± 0.04*	<0.001	11	0.98
Terrebonne	Fresh	Intertidal	CRMS 0294		0.44 ± 0.01*	<0.001	10	0.99
Terrebonne	Brackish	Intertidal	CRMS 0396		†			
Terrebonne	Saline	Intertidal	CRMS 0421		†			
Atchafalaya	Fresh	Supratidal	WLD	Belowground Biomass buried	1.22 ± 0.10*	<0.001	9	0.93
Atchafalaya	Fresh	Intertidal	WLD		0.74 ± 0.13*	<0.001	9	0.77
Atchafalaya	Brackish	Intertidal	CRMS 0399		0.58 ± 0.06*	<0.001	11	0.88
Atchafalaya	Saline	Intertidal	CRMS 0322		0.31 ± 0.02*	<0.001	10	0.93
Terrebonne	Fresh	Intertidal	CRMS 0294		1.11 ± 0.088	<0.001	9	0.95
Terrebonne	Brackish	Intertidal	CRMS 0396		†			
Terrebonne	Saline	Intertidal	CRMS 0421		†			
Atchafalaya	Fresh	Supratidal	WLD	Belowground Necromass buried	0.23 ± 0.03*	<0.001	11	0.82
Atchafalaya	Fresh	Intertidal	WLD		0.27 ± 0.02*	<0.001	11	0.94
Atchafalaya	Brackish	Intertidal	CRMS 0399		0.27 ± 0.03*	<0.001	9	0.89
Atchafalaya	Saline	Intertidal	CRMS 0322		0.16 ± 0.01*	<0.001	10	0.93
Terrebonne	Fresh	Intertidal	CRMS 0294		0.28 ± 0.02*	<0.001	10	0.95
Terrebonne	Brackish	Intertidal	CRMS 0396		0.22 ± 0.02*	<0.001	11	0.89
Terrebonne	Saline	Intertidal	CRMS 0421		0.27 ± 0.01*	<0.001	10	0.97

4. Discussion

4.1. Surface Accretion and Sedimentation Rates

The feldspar marker horizon method measures the vertical magnitude of annually surface accreted material that, along with bulk density and inorganic, organic matter, and organic carbon concentrations, can be used to quantify inorganic, organic matter, and organic carbon sedimentation rates. Soil lignin concentrations of surface accreted material can also be used to estimate the division of labile and refractory organic matter. By experimentally choosing sites delta coastal basins representing the active and inactive phase of delta cycle, and along salinity gradient in each, a comparison of surface accretion rates and sedimentation rates gives insight on the contribution of river input ot sedimentation rates on soil dynmaics in Louisiana's wetlands.

Surface accretion rates were greatest in WLD, an actively growing delta, representing proximal sedimentation in the active coastal deltaic floodplain (Twilley et al. 2019). Surface accretion in WLD was characterized by high bulk densities, low amounts organic matter, and even lower amounts of refractory organic matter (lignin). WLD feldspar stations were deployed in the center deltaic island (Mike Island) along an older and a younger chronology transect. There were significant differences between HGM zones in the younger transect , however, the older and more developed part of the island had similar surface accretion rates across HGM zones. Additionally, this older transect also had higher organic matter concentrations, suggesting both a potential equilbrium reached over time after ecological succession and a switch over time to more biological driven accretion vs. inorganic sedimentation (Aarons 2019). The younger, southern transect also had less vegetation coverage, deeper water, and greater water velocities compared to the older, northern transect, coinciding with indications of bed load transport (such

as the intertidal station being completely scoured after 12 months) (Shaw et al. 2016; Christensen et al. 2020).

Additionally, after calculating surface accretion rates by HGM for WLD sites, sedimentation rates decreased with decreasing elevation. Supratidal stations had higher surface accretion and inorganic, organic matter, and organic carbon sedimentation rates than intertidal and subtidal stations. This contradicted what I had expected based on the assumption that inorganic sedimentation rates would decrease with increased elevation due to lower frequency and duration of tidal inundation carrying suspended (Morris et al. 2020; Törnqvist et al. 2021). Although biogenic organic accretion did increase with increased elevations, inorganic sedimentation also followed the same pattern within WLD. This may be due to the great influence of the river signal at WLD as well as the size and connectivity of channels. While WLD does experience regular tides, the magnitude of the river signal dominates the landscape. Additionally, the supratidal locations in WLD are mostly found along natural levees adjacent to large distributary channels while the intertidal and subtidal interiors of the deltaic islands have shallower and smaller channels (Shaw et al. 2016). During the spring river pulse, water from the main channels overtop the natural supratidal levees and deposit large amounts of sediment, which builds these main channel levees higher overtime (Rogers 2008). Deposition decreases as distance from distributary channel increases because as water passes through vegetation and experiences frictional forces, sediment falls out of suspension and deposists, leaving less sediment in suspension to deposit in intertidal and subtidal locations that are further away from the channel. Intertidal and subtidal interior locations also experience bidirectional flow from tides, so deposited sediment can be eroded more easily in these lower elevation locations than at higher

elevation supratidal locations, also causing lower sedimentation rates (Hiatt and Passalacqua 2015).

In contrast to WLD, the other study sites were all in the intertidal HGM zone with relatively uniform marsh platform elevation typical of brackish and saline marshes (Blum 1993; Kirwan and Guntenspergen 2010). Surprisingly, the active brackish and saline sites in Fourleague Bay had the lowest surface accretion rates (1.42 cm yr^{-1}) and the highest organic matter and organic carbon densities of all the study. These two sites (CRMS 0399 and 0322) are located in the middle and lower areas east of Fourleague Bay and are expected to experience distal sedimentation from the Atchafalaya River (Twilley et al. 2019). In contrast, the brackish and saline sites in the inactive Terrebonne Bay had higher surface accretion rates of 2.03 and 2.27 cm yr^{-1}, respectively. At first it was unclear to me why the active Fourleague Bay sites would not have higher or similar surface accretion rates as the brackish and saline sites in the inactive basin since the Fourleague Bay sites are closer to a riverine source of sedimentation and have similar BGB as the Terrebonne Bay sites.

After looking at wetland platform elevation of my feldspar stations, however, there may be a simple explanation for why the active Fourleague Bay sites had less surface sedimentation. The Terrebonne Bay and Fourleague Bay study sites received either no riverine input or less than WLD sites, respectively, however, the Fourleague Bay sites were higher in elevation than Terrebonne Bay sites for both brackish and saline marshes (Figure 11). This elevation difference could explain why Fourleague Bay sites had lower surface accretion rates. These more tidal dominated intertidal marshes have a negative correlation between platform elevation and surface accretion ($R^2 = 0.41$) compared to the positive correlation found in WLD sites ($R^2 = 0.97$) (Figure 11). This negative correlation between platform elevation and surface accretion is

similarly seen in Morris et al. 2020 and Törnqvist et al. 2021. Additionally, a closer look at river stage and passing storms during our marker horizon experiment (Fall 2019 – Fall 2021) is necessary to explore if the observed surface accretion rates could be explained by discharge and winds patterns in Fourleague Bay during seasons of this study.

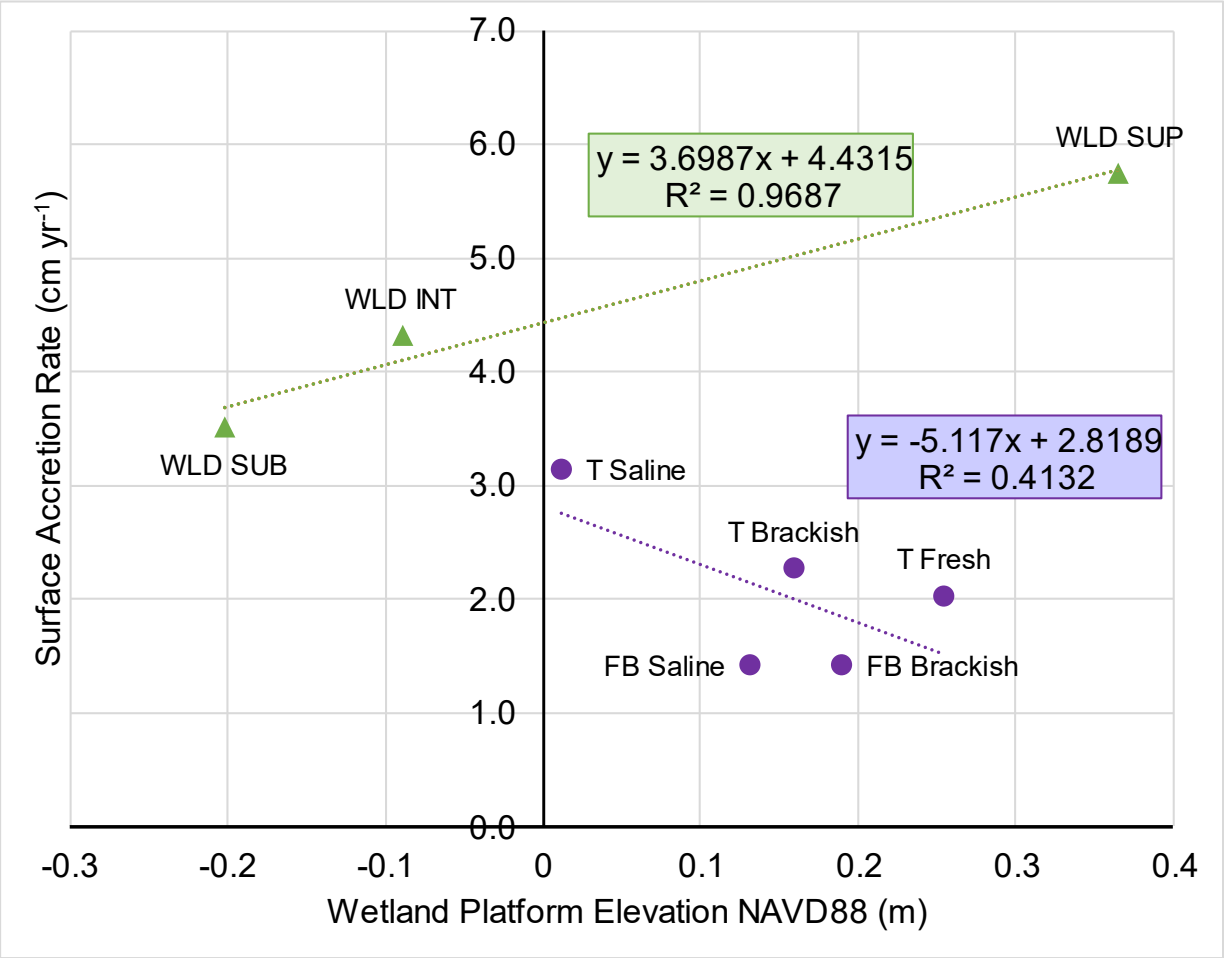

Figure 11. Average surface accretion rates (cm yr^{-1}) plotted against the average wetland platform elevation of feldspar stations at each site (NAVD88 m) with trendlines and R^2 values calculated in Microsoft Excel. Riverine dominated supratidal (SUP), intertidal (INT), and subtidal (SUB) WLD sites are shown in green triangles. More tidal dominated sites in Terrebonne Bay (T) and Fourleague Bay (FB) are shown in purple circles.

There was also a distinct trend in surface accretion rates and soil characteristics along the salinity transect in the inactive basin. As salinity increased along the transect, so did the surface accretion and inorganic and organic matter sedimentation rates. The increase of inorganic matter

with increased salinity might be due to increased tidal influence and suspended sediments being deposited on top of the marsh platform after the tide recedes (Wang et al. 1993). The amount of suspended sediment in Terrebonne Bay is sensitive to wind speed and direction during winter storms, during which there is potential for resuspension (Murray et al. 1994). Additionally, the inactive fresh site was noticably different than the other study sites in that it was flotant marsh with the greatest organic matter concentration, lowest bulk density, and greatest sediment lignin fraction of all the study sites. Flotant marshes are characterized by low bulk densities, highly organic soil, and a live root zone that floats atop a layer of water or sludge (Sasser et al. 1996). The high lignin content of the soil at this site (~30% by weight) coincides with the large amount of necromass found in collected belowground biomass cores.

4.2. Belowground Biomass and Necromass

Although belowground biomass sampling has now become standard practice in wetland sciences, belowground necromass is limited when observing and modeling these systems. As roots die and decompose, they gradually become enriched in refractory polymers, such as lignin (Benner et al. 1987; DeBusk and Reddy 1998). The structural complexity of refractory components in belowground necromass coupled with hindering anaerobic conditions of wetland soils results in slower rates of decomposition and soil organic matter accumulation (DeBusk and Reddy 1998).

Belowground biomass and necromass decomposition rates were plotted against their lignin fraction values (Figure *12*). While necromass values became clustered together on the plot, there was a negative correlation of biomass lignin and decomposition rate (increased lignin content decreases decomposition rate). Additionally, there seems to be a salinity trend following this biomass correlation. with fresh sites having lower lignin content and higher decomposition

rates compared to the brackish and saline sites (Table 2, Figure 12). Lignin content of belowground biomasss varied between sites (15-50%) while collected necromass had similar lignin content (50-60%) and similar decomposition rates across all study sites. The similarities found in the necromass suggest some physical and/or biological processes and limitations at play in wetland soils, possibly independent from vegetation type.

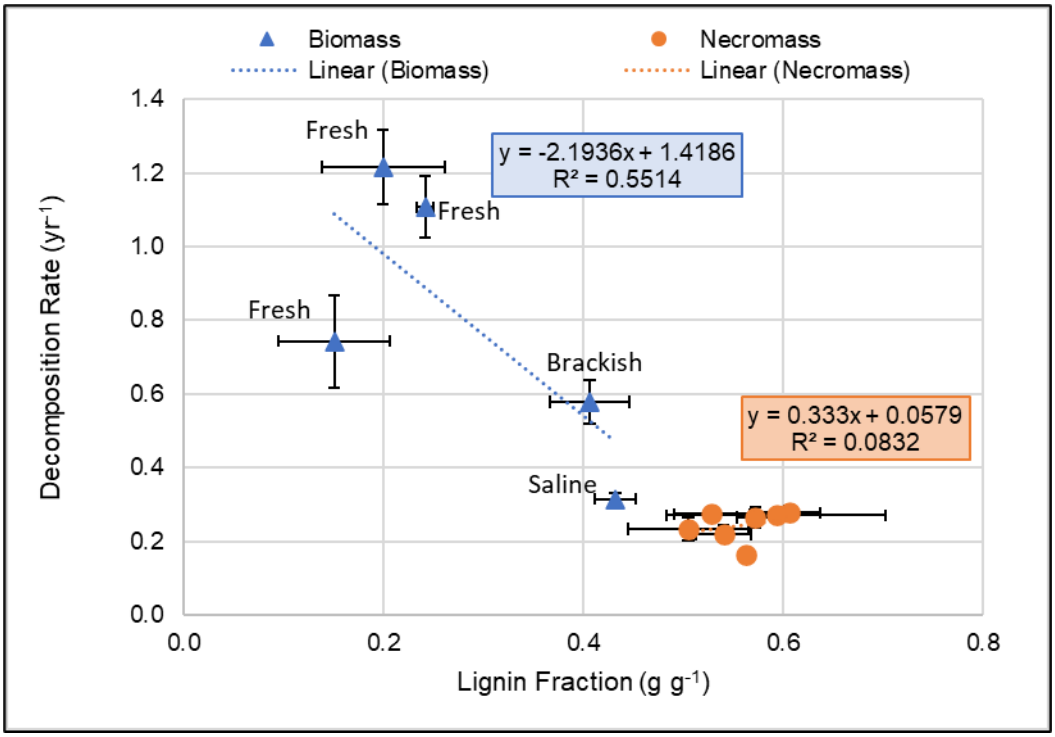

Figure 12. Mean ± standard error of lignin fraction vs. decomposition rate for both necromass (orange circles) and biomass (blue triangles) samples. Lignin values are from composite samples sent for lignin analysis (n = 3), and decomposition rates are from buried belowground biomass and necromass decomposition bags (n = 10-12). Linear trendlines (dashed lines) were added in Microsoft Excel with corresponding equations and R^2 values. Only belowground necromass decomposition rates were available for the brackish and saline sites in the inactive basin, so there are seven values for necromass but only five for biomass in the figure.

Differences between belowground biomass and necromass material matters because the amount of necromass found in the soil was significant in both active and inactive coastal basins as well across salinity gradients. Belowground necromass needs to be considered to truly capture belowground biomass dynamics. With its high refractory content, belowground necromass is

remaining in the soil for an extended amount of time, taking up a significant amount of soil volume, and is storing carbon. Whenever possible, belowground necromass should be quantified and investigated alongside belowground biomass.

5. Modeling Soil Formation

Modeling provides an opportunity to examine and test the contributions of individual components in complex processes. I modified a soil development 1-D cohort model that uses emperical data from feldspar marker horizons and collected soil and BGB samples. This model was used to explore the contribution of surface and subsurface processes in soil formation over decadal time periods. Both surface (sedimentation) and subsurface (BGB and OM decomposition) processes contribute to soil formation and thus long-term wetland sediment accretion rates. Marsh platform elevation capital is gained through this sediment accretion, and accretion helps marshes adapt to and/or counteract the effects of RSLR.

5.1 NUMAR Model Modifications

The NUMAR model is a modification of the NUMAN model by Chen and Twilley 1999. The initialization of the soil cohort layers was modified given that marshes and mangroves have different aboveground inputs (1999). The first cohort of the NUMAN model is initialized using net leaf, twig and litter production values that are informed by above ground biomass values of the mangrove forest. The largest changes to NUMAR model equations were associated with simulating herbaceous vegetation instead of mangroves. Three new equations were created to initialize each cohort with surface accretion rates from feldspar marker horizons and physicochemical characteristics of surface accreted material (Figure 13). The inorganic sedimentation rate (S_i) in g cm^{-2} yr^{-1} is described in equation (3) using the surface accretion rate (feld_a) in cm yr^{-1}, bulk density of surface accreted material (bd) in g cm^{-3}, and the inorganic fraction of surface accreted material (c1) in g g^{-1}.

$$S_i = feld\_a * bd * c_1 \quad (3)$$

The refractory organic matter (ROM) pool at time t =0 in g cm^{-2} yr^{-1} is described in equation (4) using the lignin fraction of surface accreted material (c0) in g g^{-1}.

$$\mathrm{ROM}(0) = \mathrm{feld\_a} * \mathrm{bd} * \mathrm{c}_0 \quad (4)$$

And lastly, the labile organic matter (LOM) pool at time t =0 in g cm^{-2} yr^{-1} is described in equation (5).

$$LOM(0) = feld\_a * bd * ((1 - c_1) - c_0) \quad (5)$$

Additional model changes included collapsing root production from two size classes (large and fine roots) to a single category of belowground biomass production (NUMAN eq. 7 & 8) and simplifying the amount of inorganic matter in the surface cohort (W_i) to be equal to the annual deposition of mineral sediment (S_i) without any mineral removal from surface litter production (NUMAN eq. 14) (Chen and Twilley 1999). Complete descriptions of each equation in the NUMAR model can be found in Appendix A.

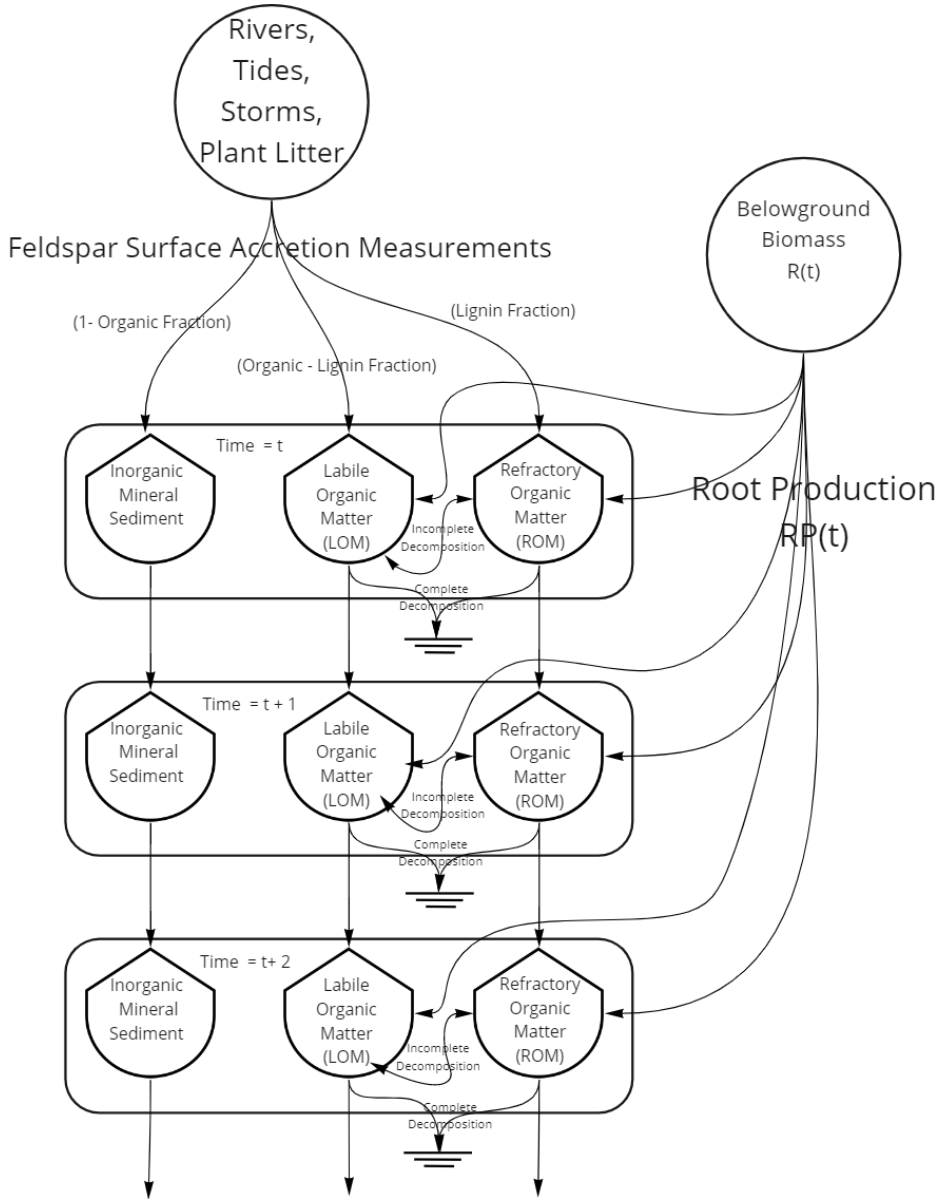

Figure 13. Conceptual diagram of NUMAR model with pools of inorganic matter, labile organic matter, and refractory organic matter in each cohort. Belowground biomass is modeled using an exponential decay function with depth (time).

The NUMAR model equations are executed using a Python script that reads an input file (.csv) with input parameters, builds and advances soil cohorts over time (ts), and outputs either 1) a full sediment profile with information from each cohort or 2) average accretion rates and soil characteristics from built sediment profile. The NUMAR python script is heavily derived from

previous work with the NUMAN model by Tom Kaiser (2016-2018) and Alex Christensen (2020) but includes my modified equations and parameters.

5.2 NUMAR Model Parameterization and Calibration

The NUMAR model has sixteen input parameters, about half of which come from empirical data that was collected in this study using methods described in previous sections. Average surface accretion rates measured using the feldspar marker horizon technique were used as the input parameter feld_a (cm yr^{-1}) (Table *1*). Mean characteristics of newly accreted material were also used as input parameters: bulk density (bd), soil inorganic fraction (c1), soil lignin fraction (c0). For each site, two model scenarios were simulated using: belowground biomass only and total root mass (biomass + necromass). The inorganic fraction (fc1) and lignin fraction (fc0) of belowground biomass were used for biomass only scenarios. For total root mass scenarios, the weighted means of necromass and biomass fractions were calculated using the ratio of biomass: necromass at each specific site (Table 2).

Two of the most important input parameters come from the site-specific belowground biomass depth-distribution curves. The intercept (R_0) and slope coefficient (e) of each site's depth-distribution curve are input parameters used to simulate root mass and belowground production in the NUMAR model. Data from collected BGB cores was used to estimate an appropriate depth-distribution curves for each site. Depth-distribution curves for WLD cores were analyzed separately for supratidal and intertidal cores. I used the average 50cm depth integrated mass (R_I) (either biomass only or total root mass) and tested different slope coefficients (e) in equation (6) – a rearrangement of the depth-distribution curve equation from the NUMAN model – to solve for intercept terms (R_0) (Chen and Twilley 1999).

$$R_0 = R_I \left[\frac{-e}{\exp(-eD) - 1}\right]$$

(6)

For each pair of tested slope and intercept terms, root mass (R) was integrated for 10cm depth intervals at 0-10, 10-20, 20-30, 30-40, and 40-50cm using equation (7) where D_t and D_b are the top and bottom depths of the modeled core sections. Equation (7) is the same equation used to model root mass in the NUMAR model, but D_b and D_t in the NUMAR model are the depths of the bottom and top of each cohort layer that vary over time.

$$R = R_0 * \exp(-eD) \rightarrow R = R_0 \int_{D_b}^{D_t} \exp(-eD) dD = R_0[\exp(-eD_b) - \exp(-eD_t)]/(-e)$$

(7)

Differences between modeled core sections and the averages of collected core sections at a site were used to provide a residual sum of squares term. Different slope coefficients (e) were tested at intervals of 0.005 (minimum of 0.001), producing different intercept terms (R_0) each time, and the slope and intercept terms that produced the least residual sum of squares were selected for each site as its depth-distribution model input parameters (Table *4*). Adding necromass increased the surface intercept parameter (R_0) and typically decreased the slope parameter or attenuation rate (e), meaning total root mass typically decreased at a slower rate with depth than biomass only (Table *4*). The R_0 and e values for each site were used as input parameters for NUMAR model runs under two scenarios: biomass only and total root mass. In model simulations, values for the active fresh intertidal site were also used for the subtidal site since BGB cores were not collected in subtidal locations.

Table 4. Results of depth-distribution curve fitting using data from collected BGB cores. Shown results for integrated root mass (R_I), the surface intercept input parameter (R_0), and the depth attenuation rate input parameter (e) are differentiated by whether they use data from biomass only or total root mass (bio+necromass). Biomass and total root mass scenarios were modeled separately for each site.

Basin	Salinity	HGM Zone	Site	Integrated Biomass to 50cm (R_I) (g cm^{-2})	Integrated Total Root Mass to 50cm (R_I) (g cm^{-2})	Biomass Surface Intercept (R_0) (g cm^{-2})	Total Root Mass Surface Intercept (R_0) (g cm^{-2})	Biomass Attenuation Rate (e) (cm^{-1})	Total Root Mass Attenuation Rate (e) (cm^{-1})
Atchafalaya	Fresh	Supratidal	WLD	0.190	0.569	0.014	0.024	0.070	0.035
Atchafalaya	Fresh	Intertidal	WLD	0.058	0.308	0.001	0.015	0.001	0.045
Atchafalaya	Brackish	Intertidal	CRMS 0399	0.282	0.708	0.014	0.020	0.045	0.015
Atchafalaya	Saline	Intertidal	CRMS 0322	0.553	1.111	0.019	0.028	0.025	0.010
Terrebonne	Fresh	Intertidal	CRMS 0294	0.612	0.710	0.006	0.015	0.001	0.001
Terrebonne	Brackish	Intertidal	CRMS 0396	0.261	0.682	0.014	0.019	0.050	0.015
Terrebonne	Saline	Intertidal	CRMS 0421	0.492	0.805	0.021	0.025	0.035	0.020

There are three decomposition rates in the NUMAR model: LOM decomposition in year 1 (k_a), LOM decomposition after year 1 (k_b), and ROM decomposition (k_c). The decomposition rates (yr^{-1}) of bags buried with belowground biomass were used as the input parameter k_b, the decomposition rate of LOM after the first year (t >1), for biomass only scenarios. For total root mass scenarios, a weighted average of decomposition rates from necromass and biomass decomposition bags was used as k_b based on the ratio of belowground biomass and necromass found at each site. The input parameter k_a, the decomposition rate of LOM during the first year (t = 1), was set to the original estimate of 0.9 yr^{-1} from the NUMAN model, and any k_b decomposition rates that were calculated above 0.9 yr^{-1} were set to 0.9 yr^{-1} for all model runs. Decomposition rates from Stagg et al. 2018 were used for the Terrebonne brackish (mesohaline) and saline (polysaline) sites where field data was missing for NUMAR model runs.

Due to the time scale of model simulations (<150 years), ROM decomposition is assumed to be minimal as refractory material by definition is takes a long time to decompose. For this reason, I chose to keep the estimated k_c value of 0.001 from the original NUMAN model, which was based on Parton et al. 1987. The self-packing bulk densities of pure organic matter (bo) and pure inorganic matter (bi) used in the model were 0.085 and 1.99 g cm^{-3}, respectively, and these values are used to calculated the bulk density and volume of each cohort based on the mass of organic and inorganic matter in each cohort (Morris et al. 2016). Root-turnover rates (k_r) from literature values in similar ecogeomorphic settings were tested in the model to determine best fit with OM and bulk density with depth data.

Sensitivity analysis was conducted for all NUMAR input parameters including ones that are difficult measure and were previously estimated in the NUMAN model (i.e. refractory organic matter (ROM) decomposition rate (k_c), the proportion of microbial respiration during

decomposition (f_2), and the fraction of incomplete decomposition flowing from LOM to ROM (f_3)). Each of the NUMAR input parameters were characterized with "low", "mild", or "high" sensitivity (Table 5). For each parameter, six different values were tested within a reasonable range of what that parameter could be. Parameter sensitivity was determined by how much output parameters of bulk density, organic matter concentration (% dry mass), and simulated sediment accretion rates changed during sensitivity testing.

Table 5. Results of sensitivity analysis for NUMAR input parameters with their definitions and units. Sensitivity was determined by how much sediment accretion rate, bulk density, and organic matter concentration (% dry mass) changed when that parameter was changed in isolation.

Parameter	Definition	Units	Sensitivity
feld_a	Surface accretion rate from feldspar marker horizon field data	cm yr^{-1}	High
bd	Bulk density of newly accreted material	g cm^{-3}	High
c0	Refractory fraction of newly accreted material (lignin fraction)	g g^{-1}	High
c1	Inorganic fraction of newly accreted material	g g^{-1}	High
R_0	Belowground biomass at the surface (depth-distribution intercept)	g cm^{-2}	High
e	Belowground biomass attenuation rate (depth-distribution slope)	cm^{-1}	High
kr	Belowground biomass turnover rate	yr^{-1}	High
ka	Decomposition of labile organic matter during year one	yr^{-1}	Mild
kb	Decomposition of labile organic matter after year one	yr^{-1}	Mild
kc	Decomposition of refractory organic matter	yr^{-1}	Mild
fc0	Refractory fraction of belowground biomass (lignin fraction)	g g^{-1}	High
fc1	Inorganic fraction of belowground biomass	g g^{-1}	Mild
f2	Proportion of microbial respiration during decomposition	g g^{-1}	Low
f3	Fraction of incomplete decomposition flowing from labile to refractory	g g^{-1}	Low

Sediment cores were collected at each site to calibrate the NUMAR model by comparing core data to model outputs of bulk density, ash free dry weight, and organic matter density. In Spring 2021, 50cm deep soil cores were collected with a Russian Peat Core (9.8cm^2) and sectioned every 2cm. Triplicate cores were collected near the two feldspar stations at each study site, and triplicate cores were collected at each of the six feldspar stations in WLD. These "Site Core" samples were stored, dried, weighed, ground, and analyzed for OM (% dry mass) in the same manner as the cryo-core accretion samples.

5.3 NUMAR Model Results

For each site, 70 year simulations were run under two scenarios using mean input parameters corresponding to either biomass values or total root mass values. A table of the input parameter values for all sites can be found in Appendix B. Model tuning was performed using the highly sensity input parameter of root turnover (k_r), and outputs of modeled cohort bulk density and ash-free dry weight (OM) were compared to measured values from collected site cores. Additionally, simulated sediment accretion rates (SAR) in cm yr^{-1} were compared to the site-specific surface accretion rates used in the model (feldspar marker horizon technique), and any model run that resulted in a simulated SAR larger than the input surface accretion rate was ignored. Turnover rates (kr) of 0.1, 0.3, 0.5, 1.0, 1.3, 1.5, and 2.0 yr^{-1} were tested for each site and each scenario (biomass and total root mass), and turnover rates that produced the best fit of OM (% dry mass) and bulk density with depth were selected for each site and scenario (Figure 14). The NUMAR model was calibrated for each study site (Figure 15, Figure 16, Figure 17, Figure 18, Figure 19, Figure 20, Figure 21, and Figure 22), and long-term (70 yr) SAR were simulated for each site for biomasss only and total root mass scenarios (Figure 23).

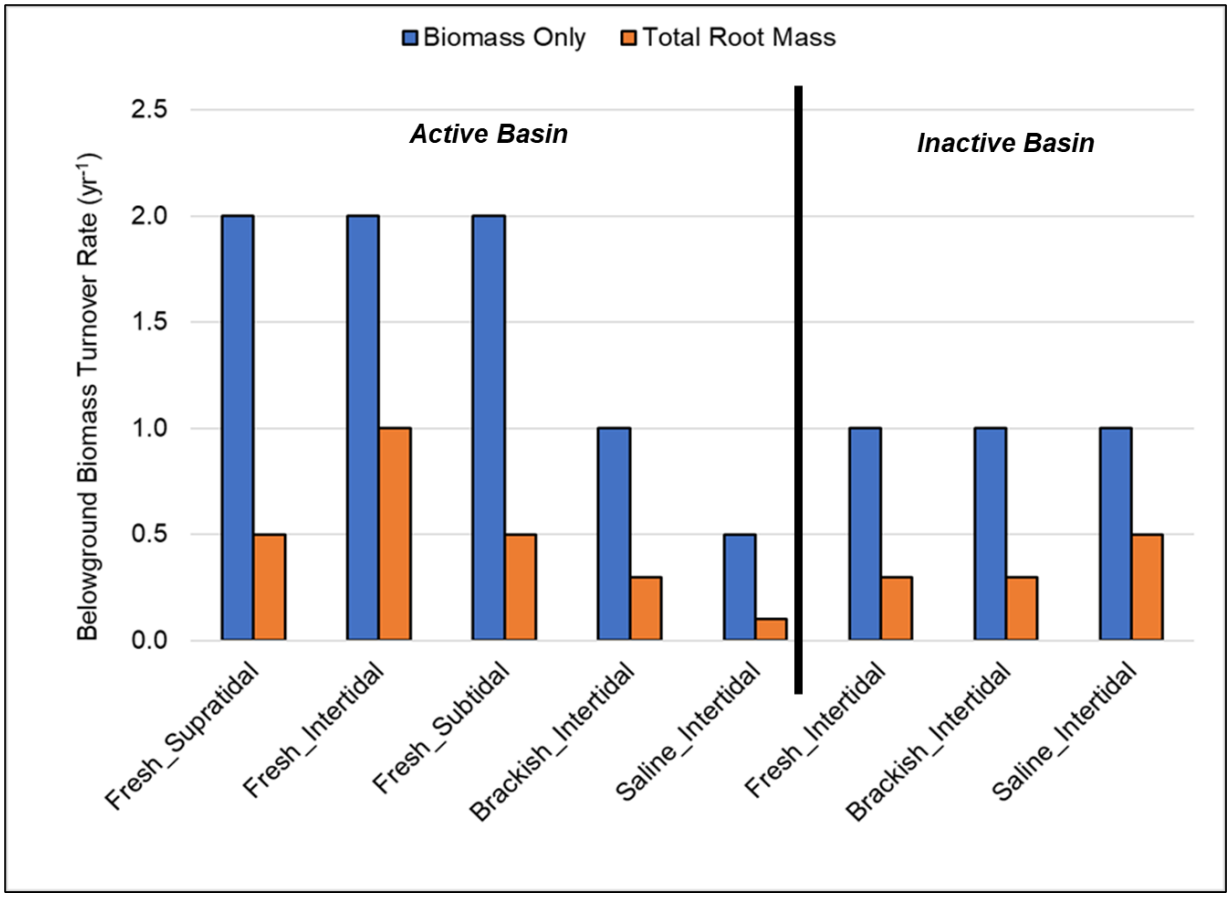

Figure 14. Belowground biomass turnover rates (k_r) used for NUMAR model runs that produced the best fit of bulk density and OM (% dry mass) with depth for each site. For both biomass only and total root mass scenarios, turnover rates of 0.1, 0.3, 0.5, 1.0, 1.3, 1.5, and 2.0 yr^{-1} were tested, and model outputs were compared to measured site core samples (50cm triplicate cores cut every 2cm). Additionally, 70-year model runs that produced sediment accretion rates greater than the input surface accretion rate from feldspar stations were ignored.

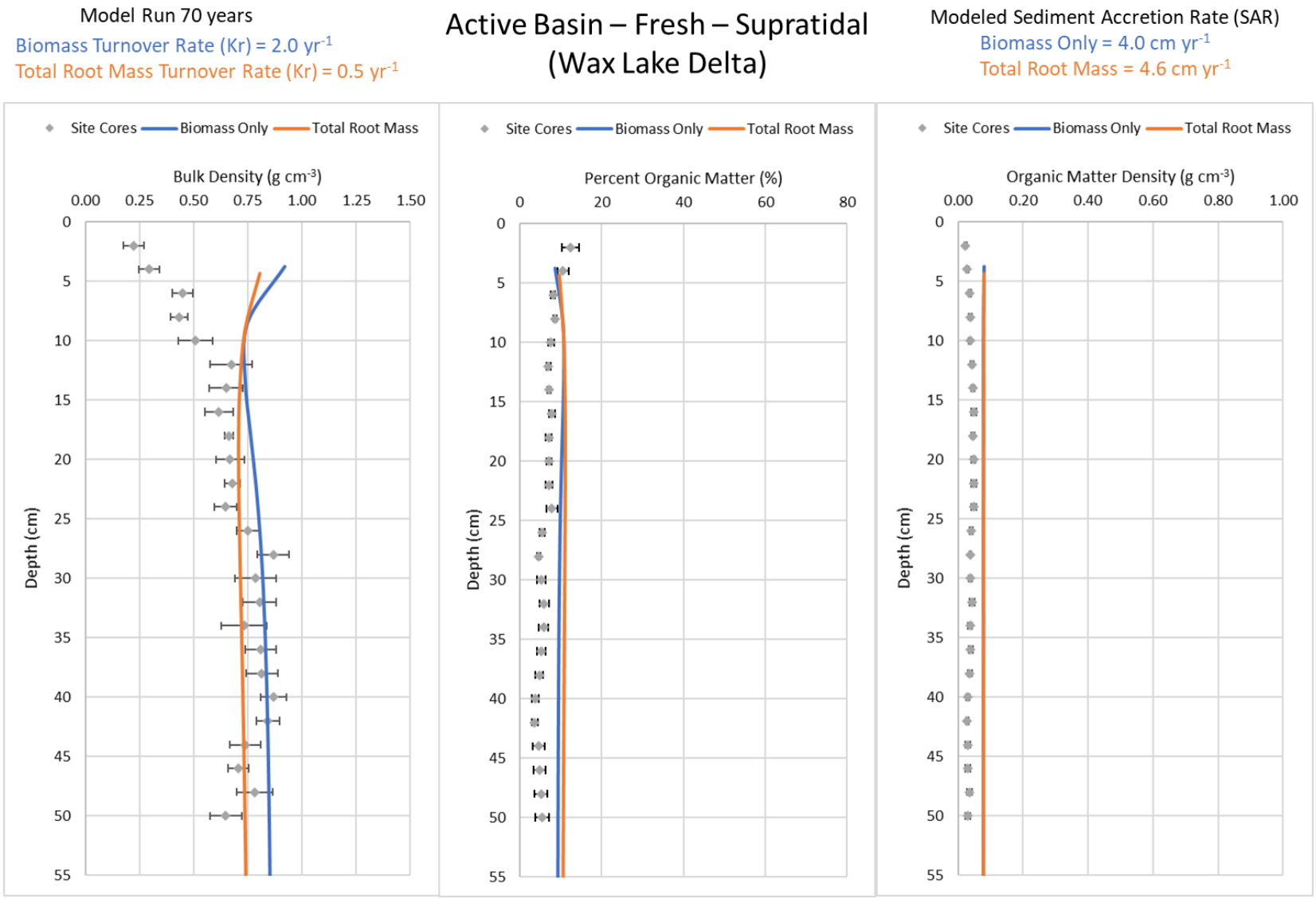

Figure 15. NUMAR model results for the active fresh supratidal site showing two scenarios using input parameters from biomass only (blue) or total root mass (orange).

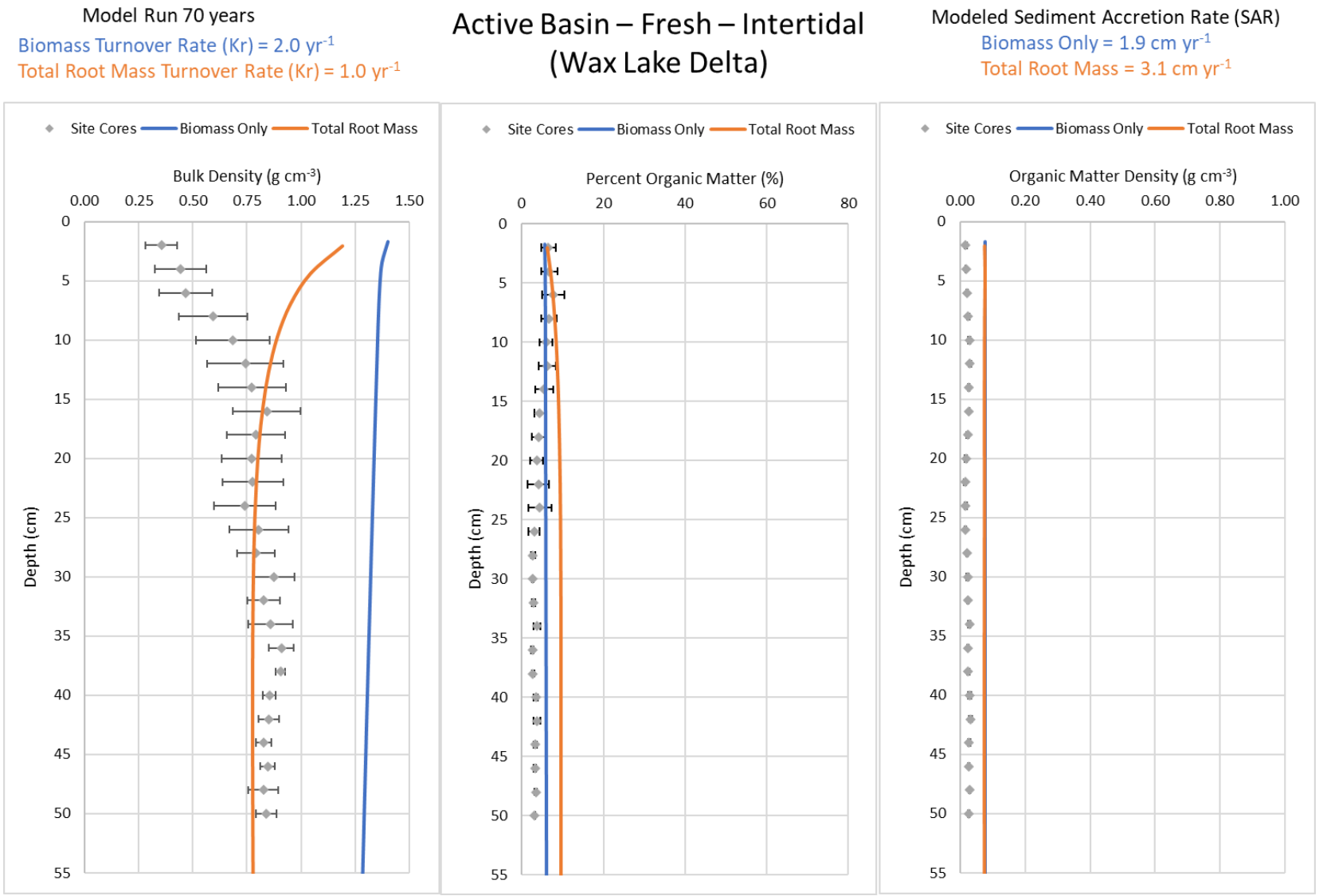

Figure 16. NUMAR model results for the active fresh intertidal site showing two scenarios using input parameters from biomass only (blue) or total root mass (orange).

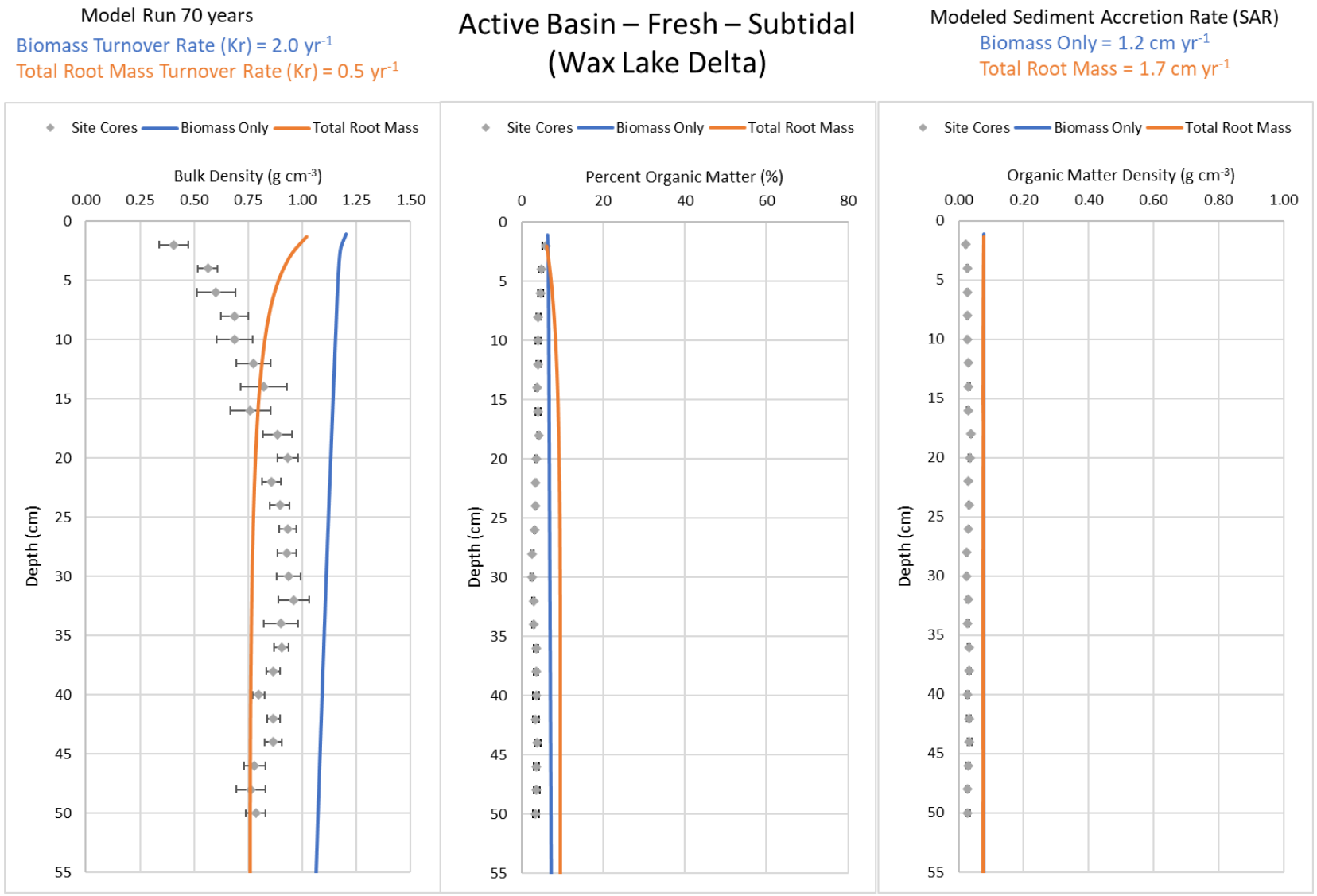

Figure 17. NUMAR model results for the active fresh subtidal site showing two scenarios using input parameters from biomass only (blue) or total root mass (orange).

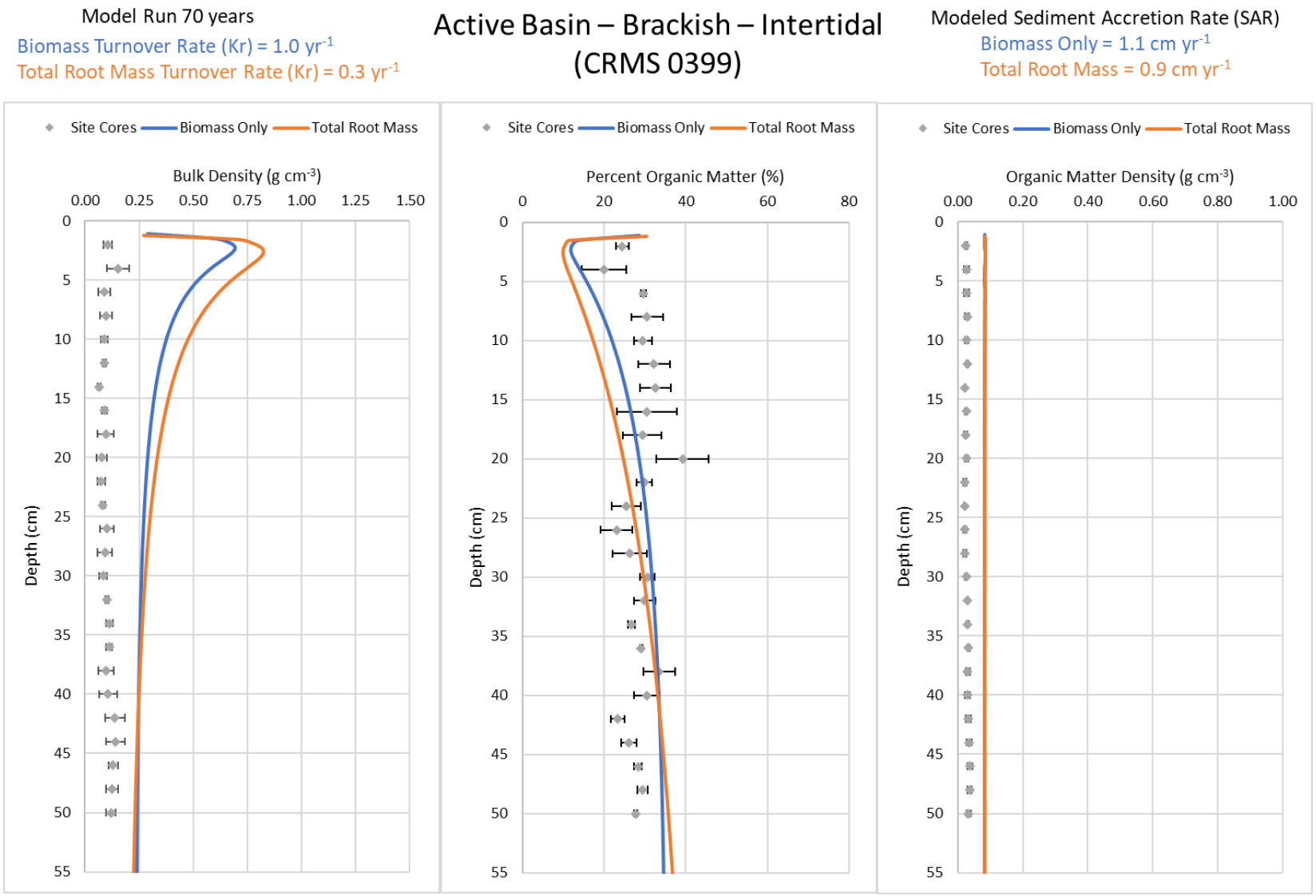

Figure 18. NUMAR model results for the active brackish intertidal site showing two scenarios using input parameters from biomass only (blue) or total root mass (orange).

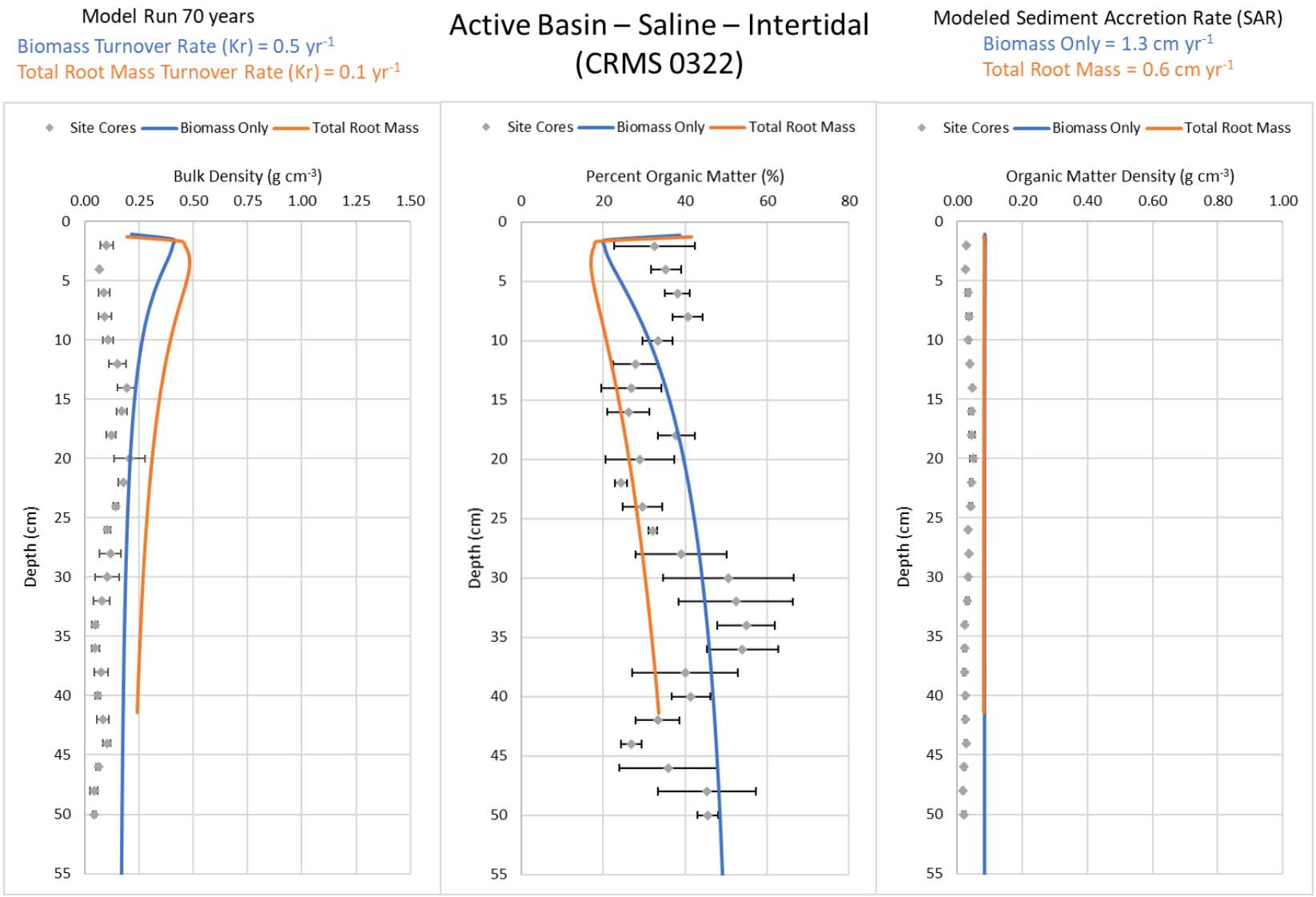

Figure 19. NUMAR model results for the active saline intertidal site showing two scenarios using input parameters from biomass only (blue) or total root mass (orange).

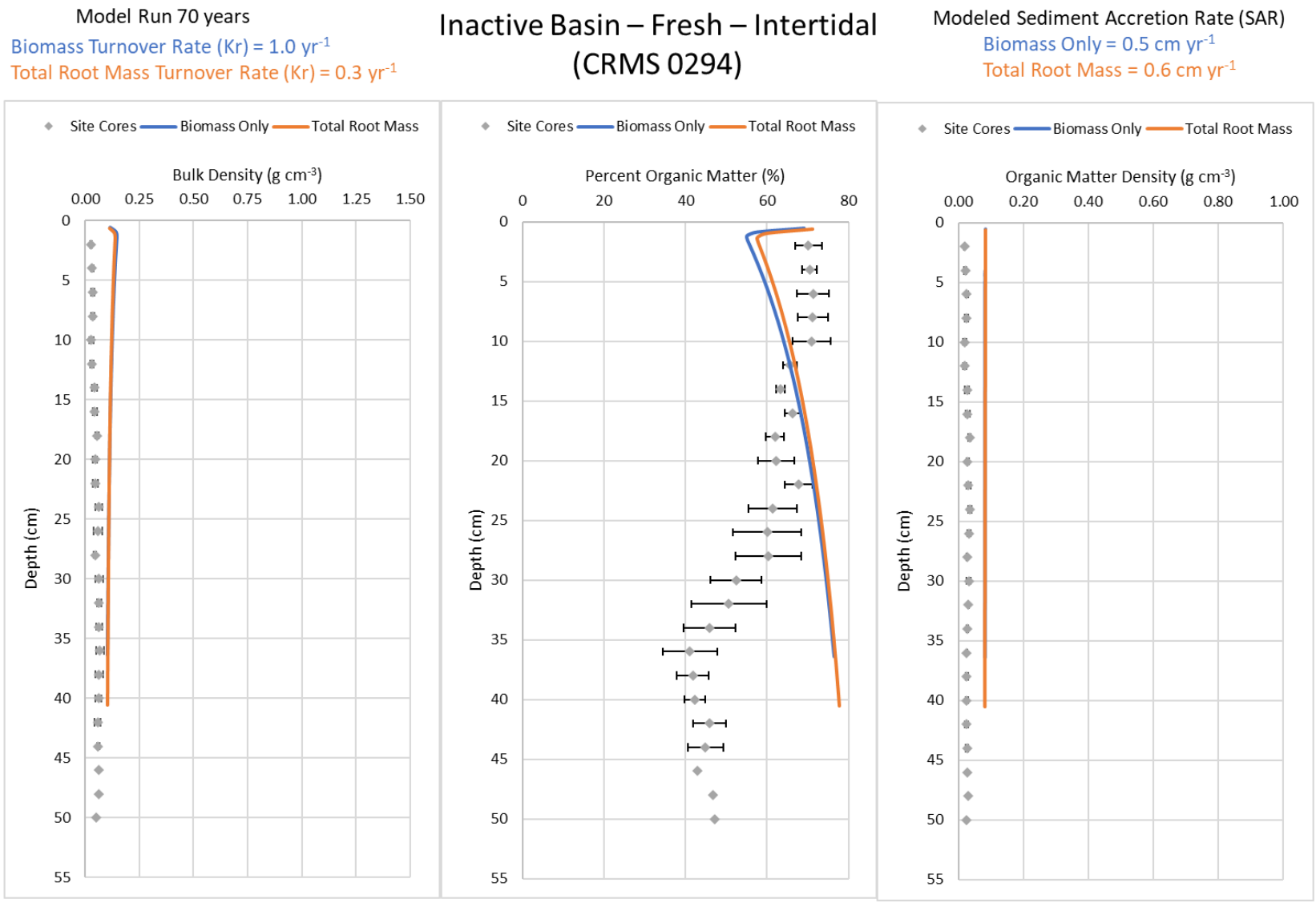

Figure 20. NUMAR model results for the inactive fresh intertidal site showing two scenarios using input parameters from biomass only (blue) or total root mass (orange).

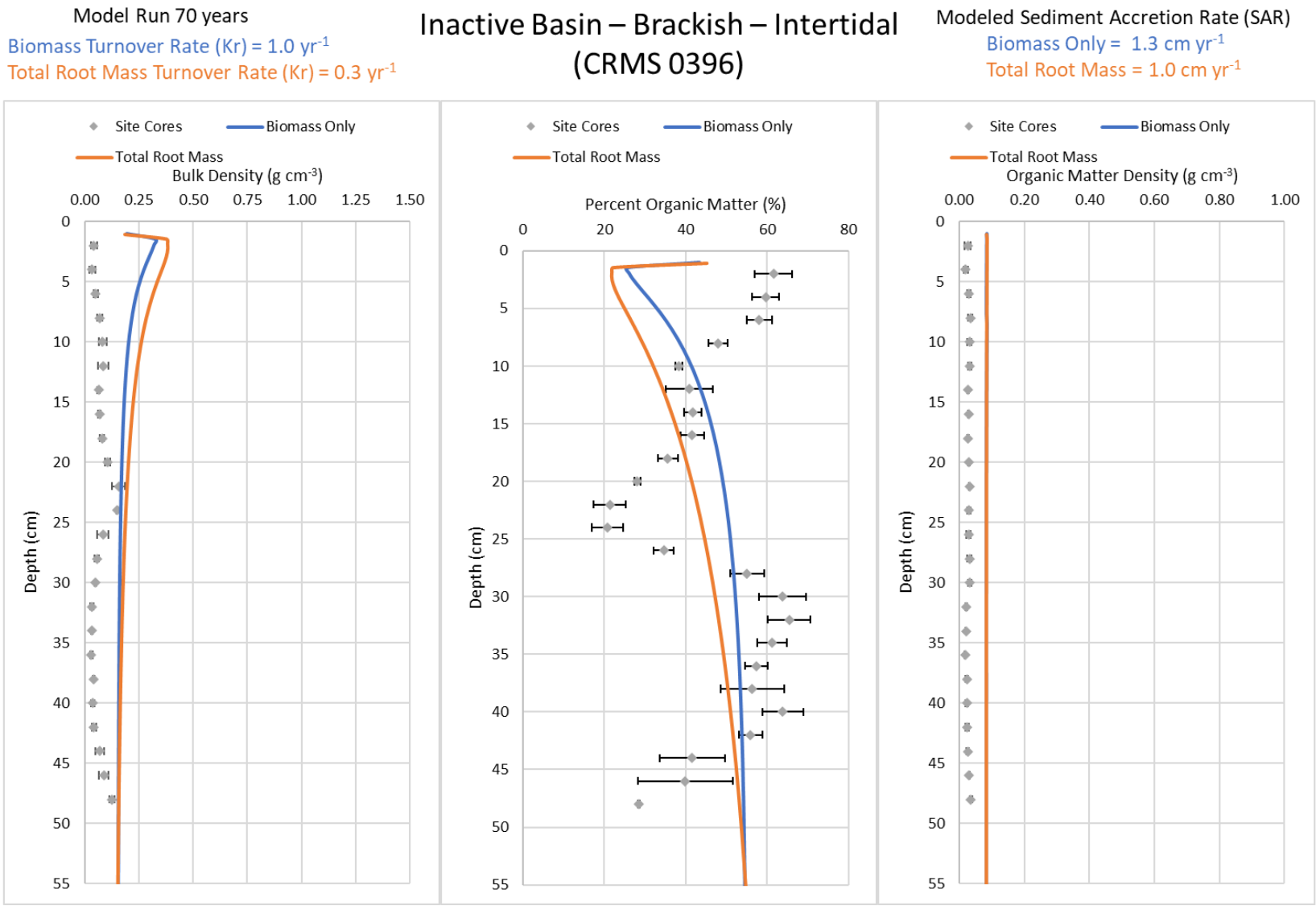

Figure 21. NUMAR model results for the inactive brackish intertidal site showing two scenarios using input parameters from biomass only (blue) or total root mass (orange).

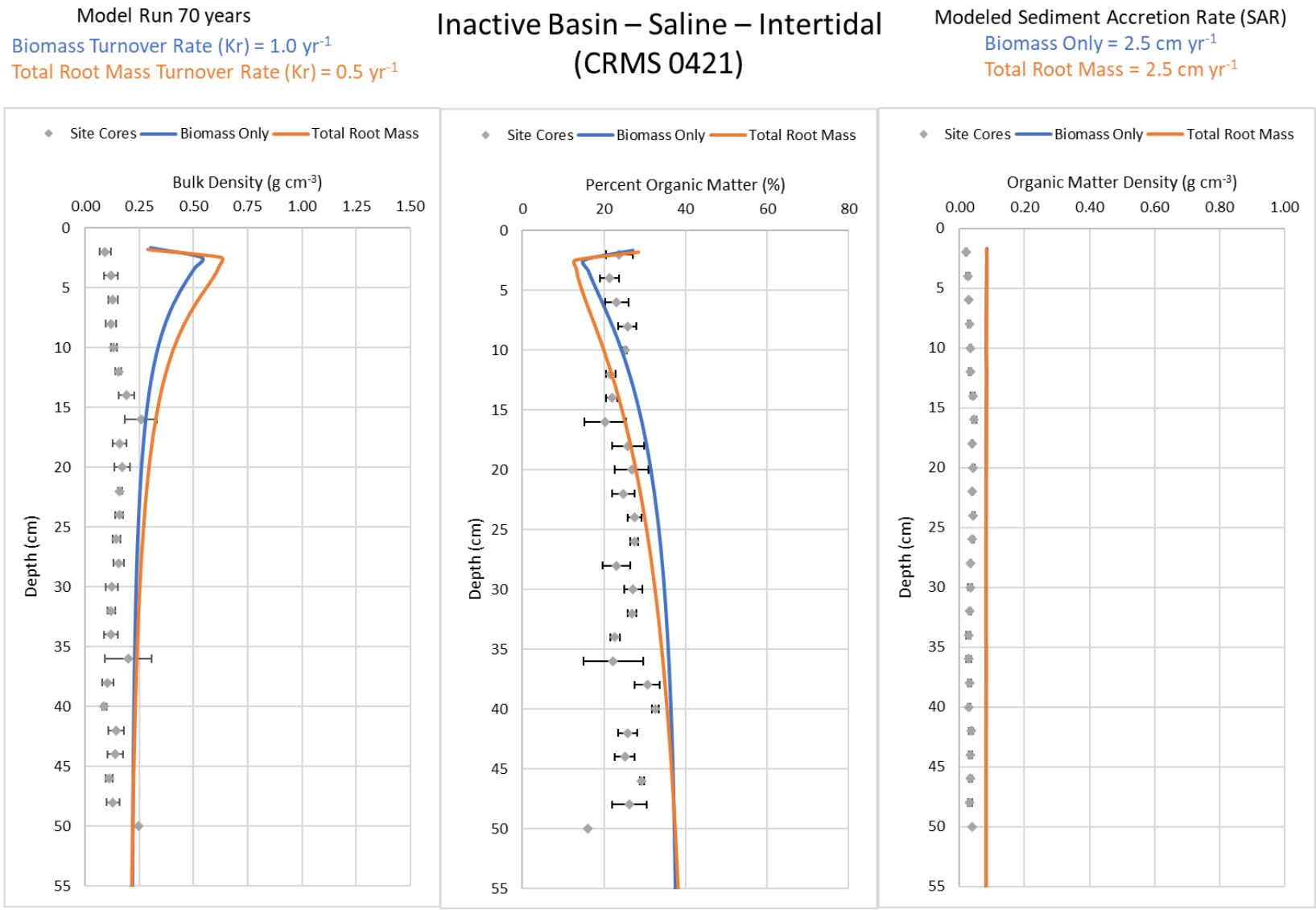

Figure 22. NUMAR model results for the inactive saline intertidal site showing two scenarios using input parameters from biomass only (blue) or total root mass (orange).

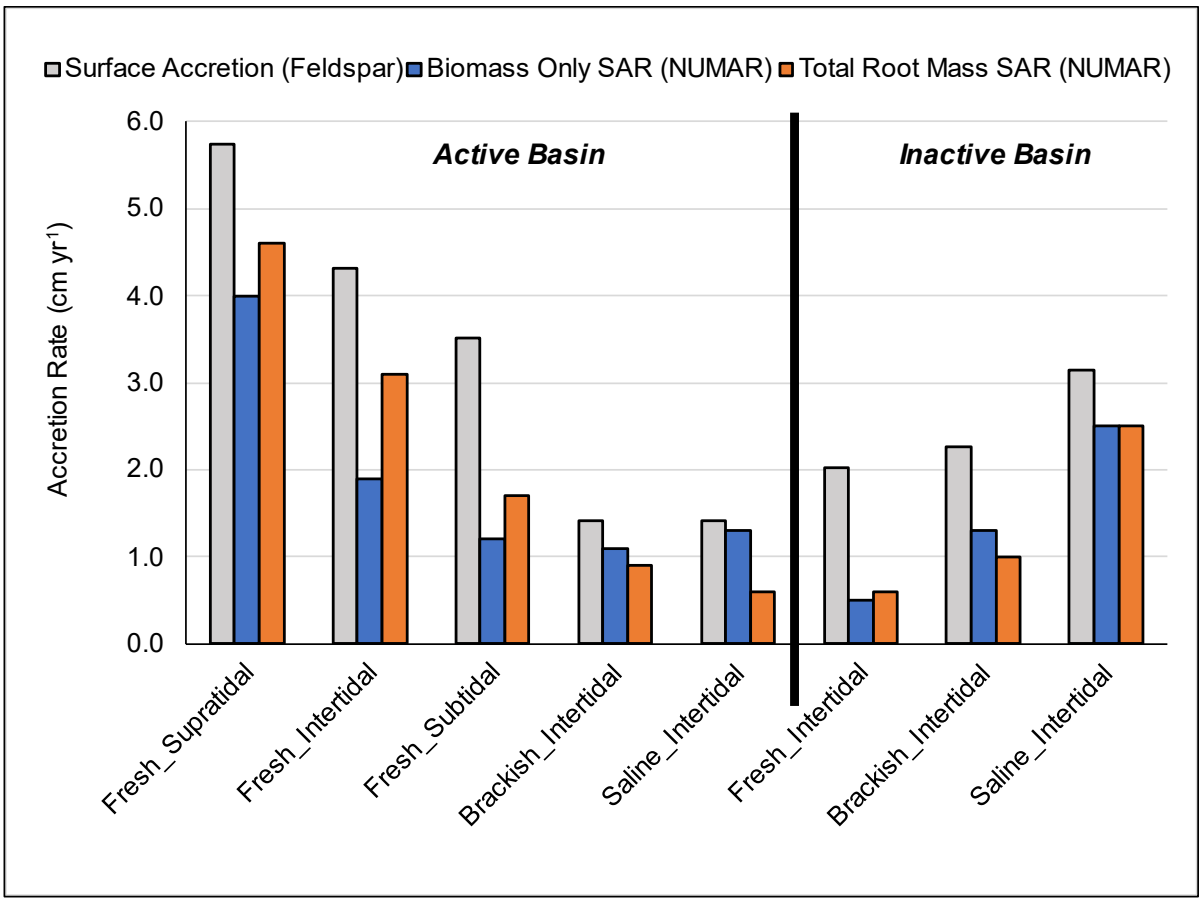

Figure 23. Surface accretion rate inputs from feldspar marker horizons compared to NUMAR simulated decadal sediment accretion rates (SAR) for biomass only and total root mass scenarios.

5.4 NUMAR Model Validation

Two brackish (CRMS 0398 and 4045) and two saline (CRMS 0377 and 4455) sites in the Terrebonne Bay (inactive basin) were used for validation. These CRMS sites were not part of the intensive study sites used to calibrate the NUMAR model. These chosen validation CRMS sites had published long-term accretion rates from Cs-137 and Pb-210 methods (Baustian et al. 2021) as well as short-term feldspar marker horizon surface accretion rates, bulk density, organic matter concentration, and belowground biomass and necromass data available (CPRA 2022). For each site's inputs, surface accretion rate (feld_a) was the average of the two most recent surface accretion rates at established CRMS feldspar stations (2018 & 2020), bulk density (bd) was the

average soil bulk density of the 0-4cm depth interval, and inorganic fraction (c1) was 100% minus the average percent organic matter of the 0-4cm depth interval (CPRA 2022). The input parameter R_0 was calculated using belowground biomass and necromass core data and slope (e) values from the brackish and saline inactive study sites (CRMS 0396 and 0421) in equation (*6*) (CPRA 2022). The remaining input parameters were values from the brackish and saline inactive study sites (c0, kr, kb, fc0, fc1), the original NUMAN model (ka, kc, f2, f3), and Morris et al. 2016 (bo, bi). A table of input parameter values for model validation runs can be found in Appendix C.

Eight NUMAR model runs were completed for model validation: two scenarios (biomass and total root mass) for four sites (CRMS 0398, 4045, 0377, and 4455). NUMAR model outputs were compared to ^{137}Cs and ^{210}Pb sediment accretion rates, OM concentration (% dry mass) with depth (0-24cm), and bulk density with depth (0-24cm) (Baustian et al. 2021; CPRA 2022). Three of the four sites had good agreement between the total root mass SAR and ^{137}Cs and ^{210}Pb accretion rates (Table *6*, Figure 24) but bulk density and OM concentration did not agree well (Figure 25, Figure 26). In contrast, the saline CRMS 0377 site severely overestimated accretion but had good agreement with bulk density and OM concentration with depth (Figure 26).

Table 6. Sediment accretion rate (SAR) results of NUMAR validation model runs compared to average cesium-137 and lead-210 accretion rates measured by Baustian et al. 2021(*).

Basin	Salinity	Site	NUMAR Biomass SAR (cm yr^{-1})	NUMAR Total Root Mass SAR (cm yr^{-1})	Cesium-137 Accretion Rate (cm yr^{-1}) *	Lead-210 Accretion Rate (cm yr^{-1}) *
Terrebonne	Brackish	CRMS 0398	0.79	0.73	0.90	0.80
Terrebonne	Brackish	CRMS 4045	1.54	0.80	0.76	0.50
Terrebonne	Saline	CRMS 0377	2.06	2.63	0.40	0.18
Terrebonne	Saline	CRMS 4455	0.63	0.93	0.80	0.79

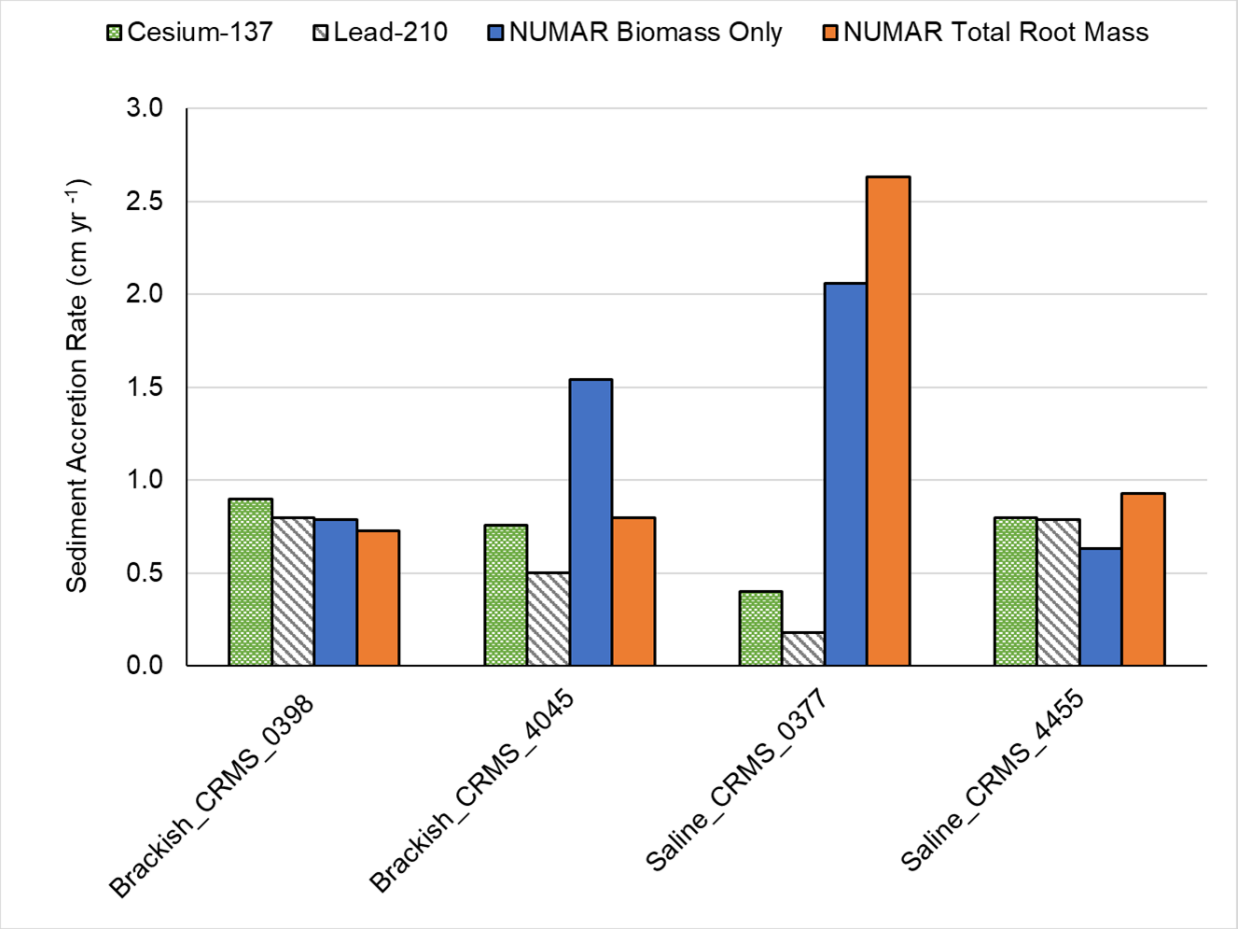

Figure 24. Comparison of decadal sediment accretion rates from either Cs-137 and Pb-210 methods (Baustian et al. 2021) or NUMAR model simulations (biomass only and total root mass scenarios) for chosen validation CRMS sites. CRMS 0398 and 4045 are brackish marshes in Terrebonne Bay, and CRMS 0377 and 4455 are saline marshes in Terrebonne Bay. Shown Cs-137 and Pb-210 rates are means measured by Baustian et al. 2021.

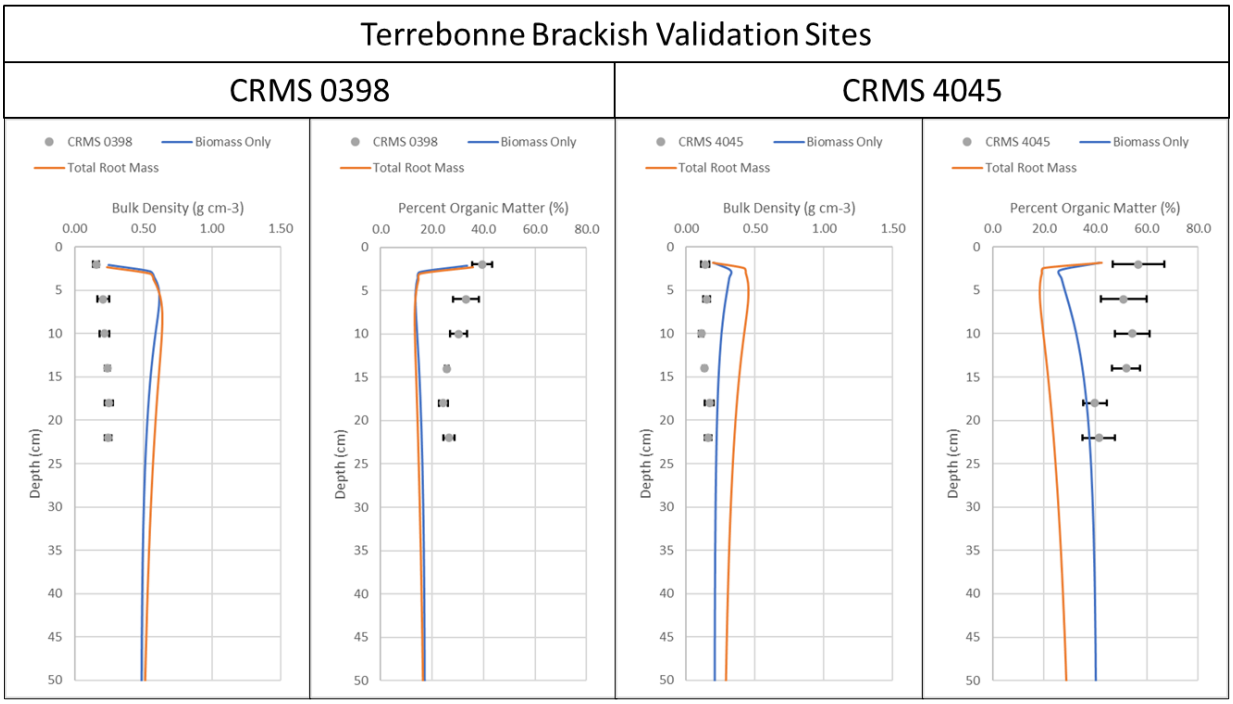

Figure 25. Bulk density and OM concentration (% dry mass) results of NUMAR model runs for Terrebonne brackish validation CRMS sites. Gray dots are core section averages from CPRA 2022.

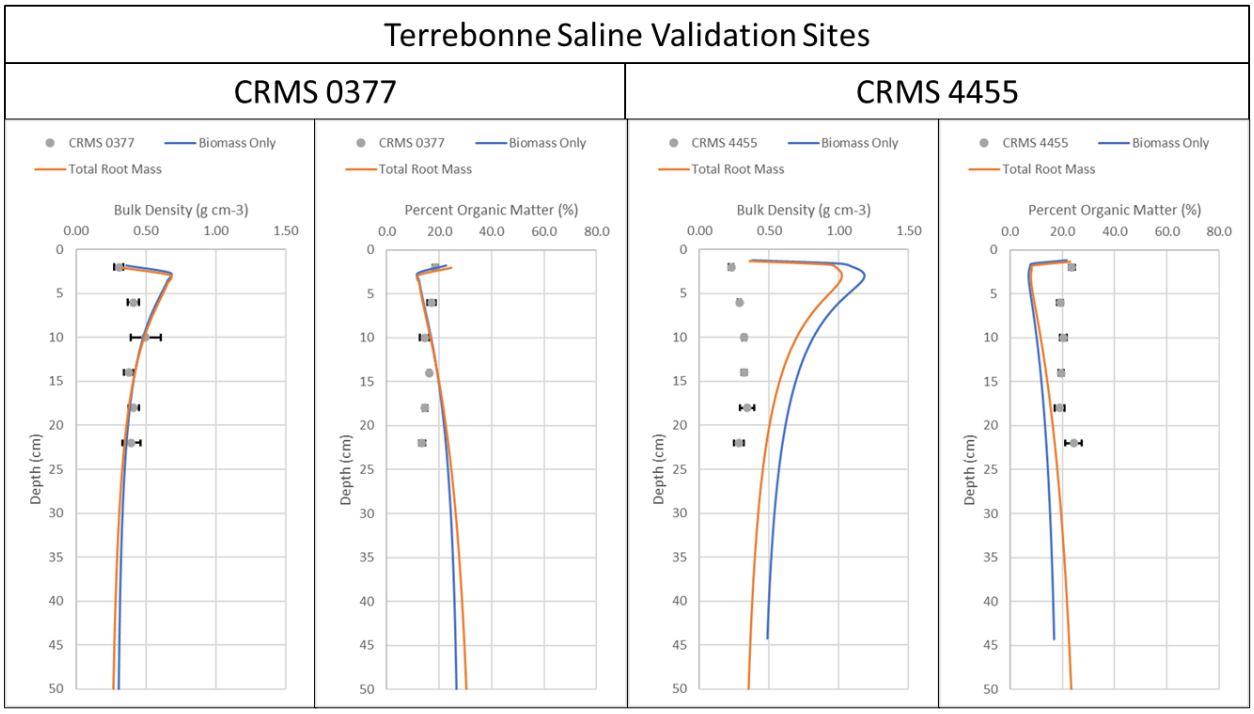

Figure 26. Bulk density and OM concentration (% dry mass) results of NUMAR model runs for Terrebonne saline validation CRMS sites. Gray dots are core section averages from CPRA 2022.

5.5 Discussion of NUMAR Model

Simulated sediment accretion rates were determined by multiple highly sensitive input parameters, including surface accretion rates (feld_a) measured by the feldspar marker horizon method (Cahoon et al. 1996; Folse et al. 2018), lignin fraction of newly accreted material (c0) and BGB (fc0), BGB turnover rate (k_r), and BGB depth distribution curves (R_0 and e). Final model results were selected if simulated SAR was less than the measured surface accretion rates, because annual surface accretion methods (such as feldspar marker horizons) overestimate vertical accretion rates when compared to longer term methods of both ^{137}Cs and ^{210}Pb (DeLaune et al. 1989; Rybczyk 1997). For each study site, measured and estimated input parameters were used in the modified NUMAR model equations to output similar organic matter (% dry mass) and bulk density results with depth as of collected site cores. In all model runs, there were large changes of bulk density and OM (% dry mass) in the surface 10cm that looked similar to model spin up before an equilibrium was reached. The same issue can be seen in results of the original NUMAN model (Chen and Twilley 1999), and results in the first 10cm should be disregarded. Best model fits of OM (% dry mass) and bulk density were found at the WLD supratidal (Figure 15). Fourleague Bay brackish and saline sites (Figure 18, Figure 19), and the saline site in Terrebonne (Figure 22). These sites had more consistent OM (% dry mass) with depth compared to the Terrebonne fresh and brackish sites (Figure 20, Figure 21).

Greatest simulated SAR were found at the active fresh sites in WLD (1.2 - 4.6 cm yr^{-1}) while lower simulated SAR were found in the inactive fresh site (0.5 and 0.6 cm yr^{-1}) (Figure 23). This large difference of SAR between coastal basins in fresh sites is most likely due to the large amount of sediment being deposited at Wax Lake Delta (3.5-5.7 cm yr^{-1} with newly accreted material >90% inorganic by mass) compared to the biologically driven accretion found

at the inactive, floating marsh site (2.0 cm yr^{-1} with newly accreted material >70% organic by mass). Although soil organic matter takes up significantly more volume than mineral matter (Morris et al. 2016), mineral matter is conserved in the soil while a portion of organic matter is decomposed. Therefore, an active delta like WLD with lots of mineral surface accretion would have similar long-term accretion rates while a highly organic fresh marsh with little sedimentation would have much lower long-term SAR (Figure 23). Brackish (1.1, 0.9 cm yr^{-1}) and saline (1.3, 0.6 cm yr^{-1}) sites in Fourleague Bay had modeled SAR that were in range of ^{137}Cs sediment accretion rates measured in the Atchafalaya basin (Baumann et al. 1984; Nyman et al. 1990; Nyman et al. 2006). Additionally, the Terrebonne brackish (1.3, 1.0 cm yr^{-1}) site had simulated SAR that fell within range of what I saw measured in coastal Louisiana. In contrast, SAR in the Terrebonne saline (2.5 cm yr^{-1}) site was quite large compared to literature I saw across coastal wetlands in Louisiana (Hatton et al. 1983; DeLaune et al. 1989; Nyman et al. 1990; Nyman et al. 1993; Milan et al. 1995; Nyman et al. 2006), which I believe to be an overestimation of the model.

Belowground biomass turnover rates of 0.1, 0.3, 0.5, 1.0, 1.3, 1.5 and 2.0 yr^{-1} were tested input variables for each site (using biomass and total root mass scenarios). These values were chosen to test because of the variability of turnover rates found in literature and the high sensitivity of this input parameter. The NUMAN model estimated a turnover rate of 0.1 yr^{-1} for mangroves (Chen and Twilley 1999) while its predecessor, the SEMIDEC model, estimated 0.5 yr^{-1} for marshes (Morris and Bowden 1986). Some measured turnover rates for *Spartina* marshes include 0.14-3.22 yr^{-1} (Schubauer and Hopkinson 1984), 0.26-0.62 yr^{-1} (Groenendijk and Vink-Lievaart 1987), 0.54-2.63 yr^{-1} (Blum 1993), 0.04-0.43 yr^{-1} (Elsey-Quirk and Unger 2018), and 0.25-2.20 yr^{-1} (From et al. 2021). Some of the variablity of these turnover rates comes from the

different methods used to calculate belowground production and standing stock as well as different field collection methods, such as in-growth bags vs. serial coring.

One study, Schubauer and Hopkinson 1984, observed the greatest turnover rates using the Smalley method, which partially accounts for seasonal cycles, and saw significant decreases in turnover rates when necromass was included with biomass in each of their four tested production estimate methods (i.e. 3.22 yr^{-1} using biomass only compared to 0.77 yr^{-1} using biomass and necromass combined = total root mass) (Smalley 1958). Another study, From et al. 2021, observed lowest turnover rates (0.25, 0.34 yr^{-1}) in 12-month in-grow bags (biomass and necromass combined) compared to serial coring methods that either included biomass and necromass (1.11, 0.92 yr^{-1}, Smalley method) or only biomass (2.17, 2.20 yr^{-1}, Max-Min method). This pattern of estimating lower turnover rates when including belowground necromass fits well with the trend I saw during model calibration. The turnover rates of model runs that produced the best fit varied by site, but, biomass only scenarios consistently needed a higher turnover rate (0.5-2.0 yr^{-1}) to fit data as well as the total root mass scenarios (0.1-1.0 yr^{-1}) which included necromass (Figure 14). Although this study combined belowground biomass and necromass into a total root mass category for modeling purposes, future work on the NUMAR model should model necromass as a separate entity with its own dynamics. However, if necromass data is not available, it is possible to parameterize the NUMAR model with biomass only parameters and get similar results. It is just important to select a larger turnover rate than you would if you accounted for necromass. This difference between turnover rates works out mathematically because BGB stocks are less than total root mass stocks, so you need a higher turnover rate for BGB to achieve the same BGB production rate in the NUMAR model and thus similar model results (BGB production = stock * turnover rate).

NUMAR Model validation was done on using four CRMS sites (2 brackish, 2 saline marshes) in the inactive Terrebonne Bay. Three of the four chosen validation sites had sediment accretion rates comparable to ^{137}Cs and ^{210}Pb accretion rates measured at each site (Baustian et al. 2021) (Table 6). However, bulk density and OM (% dry mass) did not fit as well with depth at these three sites compared to the study sites NUMAR was calibrated with. Bulk density was overestimated and OM (% dry mass) underestimated by the model compared to measured CPRA core data (CRMS 0398, 4045, and 4455) (Figure 25, Figure 26). It is also hard to tell how well the model ran because available core data only went to 24cm and model spin up makes the top ~10cm unusable. The fourth site fit bulk density and OM (% dry mass) but modeled SAR over 5x greater than measured ^{137}Cs and ^{210}Pb rates (Table 6, Figure 26). Model validation also needs to be done for sites in the Atchafalaya basin in the future, which was left out of this study's validation. Additionally, ^{137}Cs dating cores were collected at several of the study sites in Fall 2021, and sediment accretion results should be available in the coming months. These ^{137}Cs rates can then be used to further calibrate the NUMAR model before it is to be used in a landscape ecogeomorphic model for NASA's Delta-X Mission.

One noticable drawback of the NUMAR model is that compaction is not accounted for like it is in other cohort models (Callaway et al. 1996; Rybczyk et al. 1998; Swanson et al. 2014). This could explain why there were high >2.0cm yr^{-1} sediment accretion rates modeled for the Terrebone saline study site as well as the saline validation site (CRMS 0377) (Figure 23, Figure 26). Another drawback of the current NUMAR model is that it builds a sediment profile assuming that surface accretion is the same amount with the same soil characteristics each year, which is simply unrealistic in coastal wetlands. Future versions of the NUMAR model should

include a mechanism that allows the user to change the amount and/or characteristics of surface accretion input into the model for each year.

For example, the model could randomly select a surface accretion rate (feld_a parameter) each model year that is within a 95% confidence interval or within one standard error of the mean reported feldspar accretion rates. Future versions could also include an option to induce a random disturbance with some recurrence interval, such as a hurricane, river flood pulse, or winter storm, that could either scour or deposit additional sediment. This type of flexibility is necessary to make the model more realistic for several reasons: 1) surface accretion is naturally quite variable because normal sediment deposition and belowground biomass dynamics are quite variable within the same site due to connectivity and biological variance, 2) coastal Louisiana experiences extreme weather fairly frequently, which can greatly impact how much material a wetland accretes in a given year, and 3) including randomization into the model allows the user to compare multiple model runs together and leads to a more robust model (Rybczyk and Cahoon 2002; Fagherazzi et al. 2012). The pairing of the decadal SAR from the NUMAR model with subsidence and sea level rise rates would also give greater context to the different pressures these wetlands face in the future and help inform best wetland restoration and conservation practices using coastal and ecological engineering principles.

5.6 Engineering Applications of NUMAR Model

There are a few different ways that the NUMAR model could benefit coastal engineers and scientists that work in wetland restoration. The NUMAR model takes short-term surface accretion rates and estimates decadal sediment accretion rates. In a state like Louisiana, there is plenty of published feldspar marker horizon data along with the accretion records maintained by CPRA in CRMS stations. Engineers could use the NUMAR model to quickly estimate longer

term sediment accretion rates from these surface accretion measurements without needing to take sediment cores on site and pay for Cs-137 or Pb-210 dating.

Another example where NUMAR could be used is in hydrologic restoration projects, where freshwater connectivity is reestablished in the wetland and a new hydroperiod is established. Both flooding frequency and duration are known to be important to BGB production in wetland species (Morris et al. 2002; Fagherazzi et al. 2012; Kirwan and Guntenspergen 2015; Snedden et al. 2015; Rovai et al. 2022). In order to meet long-term sediment accretion rate project goal, engineers could use the NUMAR model to find an optimal BGB production that produces that goal sediment accretion rate and choose to design for a hydroperiod that achieves that level of BGB production. Another engineering application of the NUMAR model could be found in thin layer placement (TLP) restoration projects. These projects spread a thin layer of dredged sediment on top of an existing marsh platform in order to increase platform elevation. Marshes receiving TLP are typically submerging and do not have sediment accretion rates that can match pace with RSLR. For these projects, the NUMAR model could be used to illustrate how much sedimentation is needed to reach and maintain a long-term accretion rate that keeps the marsh from submerging and converting to open-water areas.

6. Conclusion

This study investigated differences in surface accretion rates and characteristics of newly accreted material in the Atchafalaya and Terrebonne basin along salinity and HGM zone gradients. Greatest surface accretion rates were found in the actively growing, river dominated WLD sites, which had a positive correlation of surface accretion and elevation (HGM zone). In contrast, more tidal dominated marsh sites had a negative correlation of surface accretion and platform elevation as higher elevations decrease the frequency and duration of flooding on top of the marsh platform, which deposits suspended sediment on top of the marsh. Bulk density and OM concentration (% dry mass) of newly accreted material differed between sites while organic matter and organic carbon densities were similar for most sites. In the inactive basin, inorganic and organic sedimentation rates increased with increased salinity while the opposite trend was found in the active basin for most parameters. Belowground biomass and necromass stocks and decomposition rates were investigated along with their lignin contents, suggesting that necromass is an important component in organic matter accumulation and soil formation as it is high in lignin content and slow to decompose.

Empirical data from this study was utilized to parameterize and calibrate the NUMAR model, a modification of the NUMAN cohort model previously used for Florida mangroves (Chen and Twilley 1999). The NUMAR model is a sediment cohort model that takes surface accretion rates from feldspar marker horizons, surface accreted soil characteristics, and belowground biomass dynamics and models decadal sediment accretion rates in marshes that comparable to ^{137}Cs dating. The model was calibrated using field data from sites in an active and inactive coastal deltaic basin across salinity and HGM gradients. Further work needs to be done to improve the NUMAR model, including further calibration and validation, modeling soil

compaction dynamics, and modeling surface accretion variability and/or disturbance. With these improvements, the NUMAR model could be used with data from the wide network of Coastwide Reference Monitoring System (CRMS) stations to further predict long-term landscape level sediment accretion rates in coastal Louisiana.This information, along with surface elevation and subsidence data, can help inform efforts in wetland restoration and management about how marsh platform elevation will change over time during restoration projects such as thin layer placement and marsh creation projects.

Appendix A. NUMAR Model Equations

1. $$Si = feld\_a * bd * c_1$$

Net Annual Inorganic Input into each cohort is equal to (accretion rate from feldspar) * (bulk density of felspar plug) * (ash fraction of feldspar plug).

Units: (g cm^{-2} yr^{-1}) = (cm yr^{-1}) * (g cm^{-3}) * (g g^{-1})

2. $$ROM(0) = feld\_a * bd * c_0$$

Refractory Organic Matter at t = 0 is equal to (accretion rate from feldspar) * (bulk density of feldspar plug) * (lignin fraction of feldspar plug).

Units: (g cm^{-2} yr^{-1}) = (cm yr^{-1}) * (g cm^{-3}) * (g g^{-1})

3. $$LOM(0) = feld\_a * bd * ((1 - c_1) - c_0)$$

Labile Organic Matter at t = 0 is equal to (accretion rate from feldspar) * (bulk density of feldspar plug) * (organic matter fraction of feldspar plug minus lignin fraction of feldspar plug).

Units: (g cm^{-2} yr^{-1}) = (cm yr^{-1}) * (g cm^{-3}) * ((g g^{-1}) – (g g^{-1}))

4. $$R = R_0 * exp(-e * D)$$

Belowground Biomass is equal to (belowground biomass at surface, depth equals zero) * natural exponent of (negative belowground biomass attenuation rate * depth).

Units: (g cm^{-2}) = (g cm^{-2}) * (cm^{-1}) * (cm)

5. $$R(t) = R_0 \int_{D_b}^{D_t} \exp(-e * D)\, dD = R_0[\exp(-e * D_b) - \exp(-e * D_t)]/(-e)$$

Belowground Biomass at time t is equal to the integrated belowground biomass between the top and bottom depths of the cohort at time t with respect to depth.

Units: (g cm^{-2}) = (g cm^{-2}) * (cm^{-1}) * (cm)

6. $$RP(t) = k_r * R(t)$$

Belowground biomass production at time t is equal to (belowground biomass turnover rate) * (belowground biomass at time t).

Units: (g cm^{-2} yr^{-1}) = (yr^{-1}) * (g cm^{-2})

7. $$\boldsymbol{LOM(t+1) = LOM(t) - k * LOM(t) + ((1 - fc_0) * RP(t) * (1 - fc_1)) + (k_c * ROM(t) * (1 - f_2))}$$

Labile Organic Matter at time t+1 is equal to (Labile Organic Matter from previous cohort at time t) minus (the decayed fraction of LOM from the previous cohort) plus (1- the lignin fraction of belowground biomass multiplied by belowground biomass production at time t multiplied by 1 minus the ash content of belowground biomass) plus (the decayed fraction of Refractory Organic Matter at time t multiplied by 1- the fraction used up in microbial respiration (complete decomposition)). Functionally, next cohort's LOM is the previous cohort's LOM minus decayed LOM plus labile portion of root production plus incomplete decomposition from ROM to LOM. Decay rate k is k_a for t < 1 and k_b for t ≥ 1.

Units: (g cm^{-2} yr^{-1}) = (g cm^{-2} yr^{-1}) – ((g g^{-1}) * (g cm^{-2} yr-1)) + ((g g^{-1}) * (g cm^{-2} yr-1) *(g g^{-1})) + ((g g^{-1}) *(g cm^{-2} yr^{-1}) * (g g^{-1}))

8. $$\boldsymbol{ROM(t+1) = ROM(t) - \left(k_c * ROM(t)\right) + \left(fc_0 * RP(t) * (1 - fc_1)\right) + (k * LOM(t) * f_3)}$$

Refractory Organic Matter at time t+1 is equal to (Refractory Organic Matter from previous cohort at time t) minus (the decayed fraction of ROM from the previous cohort) plus (the lignin fraction of belowground biomass multiplied by belowground biomass production at time t multiplied by 1 minus the ash content of belowground biomass) plus (the decayed portion of LOM at time t multiplied by the fraction of incomplete decomposition flowing from LOM to ROM). Functionally, next cohort's ROM is the previous cohort's ROM minus decayed ROM plus refractory portion of root production plus portion of LOM flowing to ROM. Decay rate k is k_a for t < 1 and k_b for t ≥ 1.

Units: (g cm^{-2} yr^{-1}) = (g cm^{-2} yr^{-1}) – ((g g^{-1}) * (g cm^{-2} yr-1)) + ((g g^{-1}) * (g cm^{-2} yr-1) *(g g^{-1})) + ((g g^{-1}) * (g cm^{-2} yr^{-1}) * (g g^{-1}))

9. $$\boldsymbol{TOM(t) = LOM(t) + ROM(t) + (R(t) * (1 - fc_1))}$$

Total Organic Matter is equal to Labile Organic Matter plus Refractory Organic Matter plus (Belowground Biomass multiplied by 1 – the ash content of below ground biomass).

Units: (g cm^{-2} yr^{-1}) = (g cm^{-2} yr^{-1}) + (g cm^{-2} yr^{-1}) +((g cm^{-2} yr^{-1}) * (g g^{-1}))

10. $$\boldsymbol{Wi(0) = Si}$$

Amount of inorganic matter in any cohort is equal to the net annual inorganic input into a cohort, derived from feldspar accretion measurements.

Units: (g cm^{-2} yr^{-1}) = (g cm^{-2} yr^{-1})

11. $$\boldsymbol{V(t) = \frac{[LOM(t)+ROM(t)+R(t)]}{bo} + \frac{Wi(t)}{bi}}$$

Volume of a one-year soil cohort at time t is equal to ((Labile Organic Matter plus Refractory Organic Matter plus Belowground biomass at time t) divided by organic bulk density) plus (inorganic matter in cohort at time t divided by inorganic bulk density (specific gravity of sand).

Units: In a year cohort: (cm) = [(g cm^{-2}) + (g cm^{-2}) + (g cm^{-2})] / (g cm^{-3}) + (g cm^{-2})/ ((g cm^{-3})

12. $$\boldsymbol{D_b = D_t + V(t)}$$

Bottom of the cohort's depth is equal to the top of the cohort's depth plus the volume of the cohort.

Units: In a year cohort: (cm) = (cm) + (cm)

13. $$\boldsymbol{BD(t) = \frac{[LOM(t)+ROM(t)+Wi(t)]}{(D_b - D_t)}}$$

Total bulk density of cohort at time t is equal to the sum of Labile Organic Matter, Refractory Organic Matter, and inorganic matter at time t divided by the height of the soil cohort at time t.

Units: In a year cohort: (g cm^{-3}) = [(g cm^{-2}) + (g cm^{-2}) + (g cm^{-2})] / (cm – cm)

14. $$\boldsymbol{AFDW(t) = \frac{TOM(t)}{[LOM(t)+ROM(t)+R(t)+Wi(t)]} * 100\%}$$

Ash free dry weight (percent organic matter) at time t is equal to the total organic matter at time t divided by (the sum of Labile Organic Matter, Refractory Organic Matter, belowground biomass and inorganic matter at time t) multiplied by 100 percent.

Units: (%) = [(g cm^{-2} yr^{-1}) + (g cm^{-2} yr^{-1})] / [(g cm^{-2} yr^{-1}) + (g cm^{-2} yr^{-1}) + (g cm^{-2} yr^{-1})] * (%)

15. $$\boldsymbol{OMD(t) = BD(t) * (\frac{AFDW(t)}{100\%})}$$

Organic matter density of a cohort a time t is equal to the bulk density at time t multiplied by (ash free dry weight divided by 100%).

Units: (g cm^{-3}) = (g cm^{-3}) * (%)

16. $$SAR\ [cm\ yr^{-1}] = \frac{D_b(ts)}{ts}$$

Model sediment accretion rate (length/time) is equal to the bottom depth of cohort at t = ts (deepest depth created in model) divided by ts (total years model run).

Units: (cm yr-1) = (cm) / (yr)

17. $$SAR\ [g\ cm^{-2} yr^{-1}] = \frac{\sum BD * V}{ts}$$

Model sediment accretion rate (mass/area/time) is equal to the bottom depth of cohort at t = ts (deepest depth created in model) divided by ts (total years model run).

Units: (cm yr^{-1}) = (cm) / (yr)

Appendix B. NUMAR Model Input Parameters for Study Sites

Basin	Salinity	HGM Zone	Scenario	feld_a	bd	c0	c1	R0	e	kr	ka	kb	kc	fc0	fc1	f2	f3	bo	bi	ts
Atchafalaya	Fresh	Supratidal	Biomass Only	5.74	0.59	0.08	0.92	0.014	0.070	2.0	0.9	0.90	0.001	0.20	0.07	0.45	0.004	0.085	1.99	70
			Total Root Mass	5.74	0.59	0.08	0.92	0.024	0.035	0.5	0.9	0.56	0.001	0.40	0.08	0.45	0.004	0.085	1.99	70
Atchafalaya	Fresh	Intertidal	Biomass Only	4.32	0.55	0.06	0.94	0.001	0.001	2.0	0.9	0.74	0.001	0.15	0.09	0.45	0.004	0.085	1.99	70
			Total Root Mass	4.32	0.55	0.06	0.94	0.015	0.045	1.0	0.9	0.36	0.001	0.46	0.13	0.45	0.004	0.085	1.99	70
Atchafalaya	Fresh	Subtidal	Biomass Only	3.51	0.37	0.07	0.93	0.001	0.001	2.0	0.9	0.74	0.001	0.15	0.09	0.45	0.004	0.085	1.99	70
			Total Root Mass	3.51	0.37	0.07	0.93	0.015	0.045	0.5	0.9	0.36	0.001	0.46	0.13	0.45	0.004	0.085	1.99	70
Atchafalaya	Brackish	Intertidal	Biomass Only	1.42	0.21	0.03	0.74	0.014	0.045	1.0	0.9	0.58	0.001	0.41	0.03	0.45	0.004	0.085	1.99	70
			Total Root Mass	1.42	0.21	0.03	0.74	0.02	0.015	0.3	0.9	0.39	0.001	0.51	0.03	0.45	0.004	0.085	1.99	70
Atchafalaya	Saline	Intertidal	Biomass Only	1.42	0.15	0.06	0.66	0.019	0.025	0.5	0.9	0.31	0.001	0.43	0.03	0.45	0.004	0.085	1.99	70
			Total Root Mass	1.42	0.15	0.06	0.66	0.028	0.010	0.1	0.9	0.24	0.001	0.50	0.04	0.45	0.004	0.085	1.99	70
Terrebonne	Fresh	Intertidal	Biomass Only	2.03	0.03	0.32	0.28	0.006	0.001	1.0	0.9	0.90	0.001	0.24	0.06	0.45	0.004	0.085	1.99	70
			Total Root Mass	2.03	0.03	0.32	0.28	0.015	0.001	0.3	0.9	0.90	0.001	0.29	0.06	0.45	0.004	0.085	1.99	70
Terrebonne	Brackish	Intertidal	Biomass Only	2.27	0.08	0.07	0.6	0.014	0.050	0.5	0.9	0.37	0.001	0.48	0.02	0.45	0.004	0.085	1.99	70
			Total Root Mass	2.27	0.08	0.07	0.6	0.019	0.015	0.1	0.9	0.28	0.001	0.52	0.02	0.45	0.004	0.085	1.99	70
Terrebonne	Saline	Intertidal	Biomass Only	3.14	0.15	0.02	0.77	0.021	0.035	1.0	0.9	0.37	0.001	0.41	0.04	0.45	0.004	0.085	1.99	70
			Total Root Mass	3.14	0.15	0.02	0.77	0.025	0.020	0.5	0.9	0.33	0.001	0.48	0.04	0.45	0.004	0.085	1.99	70

Appendix C. NUMAR Model Input Parameters for Validation Sites

Basin	Salinity	CRMS Site	Scenario	feld_a	bd	c0	c1	R0	e	kr	ka	kb	kc	fc0	fc1	f2	f3	bo	bi	ts
Terrebonne	Brackish	CRMS 0398	Biomass Only	2.63	0.19	0.07	0.68	0.009	0.05	0.5	0.9	0.37	0.001	0.48	0.02	0.45	0.004	0.085	1.99	70
			Total Root Mass	2.63	0.19	0.07	0.68	0.016	0.015	0.1	0.9	0.28	0.001	0.52	0.02	0.45	0.004	0.085	1.99	70
Terrebonne	Brackish	CRMS 4045	Biomass Only	1.55	0.2	0.07	0.66	0.027	0.05	0.5	0.9	0.37	0.001	0.48	0.02	0.45	0.004	0.085	1.99	70
			Total Root Mass	1.55	0.2	0.07	0.66	0.028	0.015	0.1	0.9	0.28	0.001	0.52	0.02	0.45	0.004	0.085	1.99	70
Terrebonne	Saline	CRMS 0377	Biomass Only	1.74	0.36	0.03	0.8	0.017	0.035	1	0.9	0.37	0.001	0.41	0.04	0.45	0.004	0.085	1.99	70
			Total Root Mass	1.74	0.36	0.03	0.8	0.024	0.02	0.5	0.9	0.33	0.001	0.48	0.04	0.45	0.004	0.085	1.99	70
Terrebonne	Saline	CRMS 4455	Biomass Only	1.84	0.25	0.03	0.79	0.007	0.035	1	0.9	0.37	0.001	0.41	0.04	0.45	0.004	0.085	1.99	70
			Total Root Mass	1.84	0.25	0.03	0.79	0.013	0.02	0.5	0.9	0.33	0.001	0.48	0.04	0.45	0.004	0.085	1.99	70

References

Aarons, Anika Abena. 2019. Spatial and temporal patterns of ecological succession and land development along a coastal deltaic floodplain chronosequence. Louisiana State University.

Allen, J. R.L. 2000. Morphodynamics of Holocene salt marshes: a review sketch from the Atlantic and Southern North sea coasts of Europe. *Quaternary Science Reviews* 19: 1555–1231. https://doi.org/10.1016/S0277-3791(00)00157-8.

Appleby, P. G., and F. Oldfield. 1978. The calculation of lead-210 dates assuming a constant rate of supply of unsupported 210Pb to the sediment. *Catena* 5: 1–8. https://doi.org/10.1016/S0341-8162(78)80002-2.

Bärlocher, Felix. 2005. Leaf mass loss estimated by litter bag technique. *Methods to Study Litter Decomposition: A Practical Guide*: 37–42. https://doi.org/10.1007/1-4020-3466-0_6.

Baumann, Robert H, John W Day, Carolyn A Miller, Source Science, New Series, and No Jun. 1984. Mississippi Deltaic Wetland Survival : Sedimentation Versus Coastal Submergence Published by : American Association for the Advancement of Science Stable URL : https://www.jstor.org/stable/1692428 224: 1093–1095.

Baustian, Melissa M., Camille L. Stagg, Carey L. Perry, Leland C. Moss, and Tim J.B. Carruthers. 2021. Long-Term Carbon Sinks in Marsh Soils of Coastal Louisiana are at Risk to Wetland Loss. *Journal of Geophysical Research: Biogeosciences* 126. https://doi.org/10.1029/2020JG005832.

Benner, Ronald, Marilyn L Fogel, and E Kent Sprague. 1987. Diagenesis of belowground biomass of Spartina alterniflora in salt-marsh sediments 36: 1358–1374.

Benner, Ronald, Patrick G. Hatcher, and John I. Hedges. 1990. Early diagenesis of mangrove leaves in a tropical estuary: Bulk chemical characterization using solid-state 13C NMR and elemental analyses. *Geochimica et Cosmochimica Acta* 54: 2003–2013. https://doi.org/10.1016/0016-7037(90)90268-P.

Bevington, Azure E., and Robert R. Twilley. 2018. Island Edge Morphodynamics along a Chronosequence in a Prograding Deltaic Floodplain Wetland. *Journal of Coastal Research* 344: 806–817. https://doi.org/10.2112/jcoastres-d-17-00074.1.

Blum, Linda K. 1993. Spartina alterniflora root dynamics in a Virginia marsh. *Marine Ecology Progress Series* 102: 169–178.

Breithaupt, Joshua L., Joseph M. Smoak, Robert H. Byrne, Matthew N. Waters, Ryan P. Moyer, and Christian J. Sanders. 2018. Avoiding timescale bias in assessments of coastal wetland vertical change. *Limnology and Oceanography* 63: S477–S495. https://doi.org/10.1002/lno.10783.

Brinson, Mark M, Ariel E Lugo, and Sandra Brown. 1981. Primary Productivity , Decomposition

and Consumer Activity in Freshwater Wetlands Author (s): Mark M . Brinson , Ariel E . Lugo and Sandra Brown Source : Annual Review of Ecology and Systematics , 1981 , Vol . 12 (1981), pp . 123-161 Published by : An 12: 123–161.

Cahoon, Donald R., James C. Lynch, and Ronald M. Knaus. 1996. Improved cryogenic coring device for sampling wetland soils. *Journal of Sedimentary Research* 66: 1025–1027. https://doi.org/10.2110/jsr.66.1025.

Cahoon, Donald R., James C. Lynch, Charles T. Roman, John Paul Schmit, and Dennis E. Skidds. 2019. Evaluating the Relationship Among Wetland Vertical Development, Elevation Capital, Sea-Level Rise, and Tidal Marsh Sustainability. *Estuaries and Coasts* 42. Estuaries and Coasts: 1–15. https://doi.org/10.1007/s12237-018-0448-x.

Cahoon, Donald R., Denise J. Reed, and John W. Day. 1995. Estimating shallow subsidence in microtidal salt marshes of the southeastern United States: Kaye and Barghoorn revisited. *Marine Geology* 128: 1–9. https://doi.org/10.1016/0025-3227(95)00087-F.

Callaway, J C, J A Nyman, and R D DeLaune. 1996. Sediment accretion in coastal wetlands: A review and a simulation model of processes. *Current Topics in Wetland Biogeochemistry* 2: 2–23.

Castañeda, Edward. 2010. Landscape patterns of community structure, biomass and net primary productivity of mangrove forests in the Florida Coastal Everglades as a function of resources, regulators, hydroperiod, and hurricane disturbance. *PhD dissertation, Louisiana State University*.

Chen, Ronghua, and Robert R. Twilley. 1999. A simulation model of organic matter and nutrient accumulation in mangrove wetland soils. *Biogeochemistry* 44: 93–118. https://doi.org/10.1007/BF00993000.

Christensen, Alexandra, Robert R. Twilley, Clinton S. Willson, and Edward Castañeda-Moya. 2020. Simulating hydrological connectivity and water age within a coastal deltaic floodplain of the Mississippi River Delta. *Estuarine, Coastal and Shelf Science* 245. https://doi.org/10.1016/j.ecss.2020.106995.

Cormier, Nicole, Robert R. Twilley, Katherine C. Ewel, and Ken W. Krauss. 2015. Fine root productivity varies along nitrogen and phosphorus gradients in high-rainfall mangrove forests of Micronesia. *Hydrobiologia* 750: 69–87. https://doi.org/10.1007/s10750-015-2178-4.

Couvillion, Brady R., Holly Beck, Donald Schoolmaster, and Michelle Fischer. 2017. Land Area Change in Coastal Louisiana (1932 to 2016) Scientific Investigations Map 3381. *U.S. Geological Survey Scientific Investigations Map 3381*: 16.

CPRA. 2022. Coastal Protection and Restoration Authority (CPRA) of Louisiana. 2022. Coastwide Reference Monitoring System-Wetlands Monitoring Data. Retrieved from Coastal Information Management System (CIMS) database. http://cims.coastal.louisiana.gov. Accessed May 1.

Davies, Brian E. 1974. Loss-on-Ignition as an Estimate of Soil Organic Matter. *Soil Science Society of America Journal* 38: 150–151. https://doi.org/10.2136/sssaj1974.03615995003800010046x.

Day, John W., G. Paul Kemp, Denise J. Reed, Donald R. Cahoon, Roelof M. Boumans, Joseph M. Suhayda, and Robert Gambrell. 2011. Vegetation death and rapid loss of surface elevation in two contrasting Mississippi delta salt marshes: The role of sedimentation, autocompaction and sea-level rise. *Ecological Engineering* 37. Elsevier B.V.: 229–240. https://doi.org/10.1016/j.ecoleng.2010.11.021.

DeBusk, W. F., and K. R. Reddy. 1998. Turnover of Detrital Organic Carbon in a Nutrient-Impacted Everglades Marsh. *Soil Science Society of America Journal* 62: 1460–1468. https://doi.org/10.2136/sssaj1998.03615995006200050045x.

Delaune, R. D., R. H. Baumann, and J. G. Gosselink. 1983. Relationships among vertical accretion, coastal submergence and erosion in a Louisiana Gulf Coast marsh. *Journal of Sedimentary Petrology* 53: 147–157. https://doi.org/10.1306/212F8175-2B24-11D7-8648000102C1865D.

Delaune, R. D., W. H. Patrick, and R. J. Buresh. 1978. Sedimentation rates determined by 137Cs dating in a rapidly accreting salt marsh [12]. *Nature* 275: 532–533. https://doi.org/10.1038/275532a0.

DeLaune, R. D., James H. Whitcomb, W. H. Patrick, John H. Pardue, and S. R. Pezeshki. 1989. Accretion and Canal Impacts in a Rapidly Subsiding Wetland. I. 137 Cs and 210 Pb Techniques. *Estuaries* 12: 247. https://doi.org/10.2307/1351904.

DeLaune, R. D., and J. R. White. 2012. Will coastal wetlands continue to sequester carbon in response to an increase in global sea level?: A case study of the rapidly subsiding Mississippi river deltaic plain. *Climatic Change* 110: 297–314. https://doi.org/10.1007/s10584-011-0089-6.

Elsey-Quirk, Tracy, and Viktoria Unger. 2018. Geomorphic influences on the contribution of vegetation to soil C accumulation and accretion in Spartina alterniflora marshes. *Biogeosciences* 15: 379–397. https://doi.org/10.5194/bg-15-379-2018.

Fagherazzi, Sergio, Matthew L. Kirwan, Simon M. Mudd, Glenn R. Guntenspergen, Stijn Temmerman, Andrea D'Alpaos, Johan Van De Koppel, et al. 2012. Numerical models of salt marsh evolution: Ecological, geomorphic, and climatic factors. *Reviews of Geophysics* 50: 1–28. https://doi.org/10.1029/2011RG000359.

Fitzgerald, S M. 1998. The development and sand body geometry of the wax lake outlet delta, Atchafalaya bay, Louisiana. *Department of Oceanography and Coastal Sciences*. Louisiana State University.

Folse, Todd M, Jonathan L West, Melissa K Hymel, John P Troutman, Anne Sharp, Dona Weifenbach, Tommy Mcginnis, and Laurie B Rodrigue. 2018. a Standard Operating Procedures Manual for the Coast-Wide Reference Monitoring System- Wetlands :

From, Andrew S., Ken W. Krauss, Gregory B. Noe, Nicole Cormier, Camille L. Stagg, Rebecca F. Moss, and Julie L. Whitbeck. 2021. Belowground productivity varies by assessment technique, vegetation type, and nutrient availability in tidal freshwater forested wetlands transitioning to marsh. *PLoS ONE* 16: 1–24. https://doi.org/10.1371/journal.pone.0253554.

Giraldo Sánchez, Beatriz. 2005. Belowground productivity of mangrove forests in southwest Florida. *PhD dissertation, Louisiana State University*.

Groenendijk, A. M., and M. A. Vink-Lievaart. 1987. Primary production and biomass on a Dutch salt marsh: emphasis on the below-ground component. *Vegetatio* 70: 21–27. https://doi.org/10.1007/BF00040754.

Harris, David, William R. Horwáth, and Chris van Kessel. 2001. Acid fumigation of soils to remove carbonates prior to total organic carbon or CARBON-13 isotopic analysis. *Soil Science Society of America Journal* 65: 1853–1856. https://doi.org/10.2136/sssaj2001.1853.

Hatton, R. S., R. D. DeLaune, and W. H. Patrick. 1983. Sedimentation, accretion, and subsidence in marshes of Barataria Basin, Louisiana. *Limnology and Oceanography* 28: 494–502. https://doi.org/10.4319/lo.1983.28.3.0494.

Hiatt, Matthew, and Paola Passalacqua. 2015. Hydrological connectivity in river deltas: The first-order importance of channel-island exchange. *Water Resources Research* 51: 2264–2282. https://doi.org/10.1002/2014WR016149.

Hudson, Paul. 2005. Deltas. In *Encyclopedia of Water Science, Second Edition (Print Version)*, ed. S. W. Trimble, B. A. Steward, and T. A. Howell, 2nd editio, 152–156. Simon and Francis. https://doi.org/10.1201/NOE0849396274.ch38.

Jensen, Daniel, Kyle C. Cavanaugh, Marc Simard, Alexandra Christensen, Andre Rovai, and Robert Twilley. 2021. Aboveground biomass distributions and vegetation composition changes in Louisiana's Wax Lake Delta. *Estuarine, Coastal and Shelf Science* 250. Elsevier Ltd: 107139. https://doi.org/10.1016/j.ecss.2020.107139.

Kirwan, Matthew L., and Glenn R. Guntenspergen. 2010. Influence of tidal range on the stability of coastal marshland. *Journal of Geophysical Research: Earth Surface* 115: 1–11. https://doi.org/10.1029/2009jf001400.

Kirwan, Matthew L., and Glenn R. Guntenspergen. 2015. Response of plant productivity to experimental flooding in a stable and a submerging marsh. *Ecosystems* 18: 903–913. https://doi.org/10.1007/s10021-015-9870-0.

Knaus, R. M., and D. R. Cahoon. 1990. Improved cryogenic coring device for measuring soil accretion and bulk density. *Journal of Sedimentary Research* 60: 622–623. https://doi.org/10.1306/212f9214-2b24-11d7-8648000102c1865d.

Lane, Robert R., Christopher J. Madden, John W. Day, and Darrell J. Solet. 2011. Hydrologic and nutrient dynamics of a coastal bay and wetland receiving discharge from the Atchafalaya river. *Hydrobiologia* 658: 55–66. https://doi.org/10.1007/s10750-010-0468-4.

Madden, Christopher J., John W. Day, and John M. Randall. 1988. Freshwater and marine coupling in estuaries of the Mississippi River deltaic plain. *Limnology and Oceanography* 33: 982–1004. https://doi.org/10.4319/lo.1988.33.4part2.0982.

Middleton, Beth A. 2020. Trends of litter decomposition and soil organic matter stocks across forested swamp environments of the southeastern US. *PLoS ONE* 15: 1–23. https://doi.org/10.1371/journal.pone.0226998.

Milan, C. S., E. M. Swenson, R. E. Turner, and J. M. Lee. 1995. Assessment of the 137Cs method for estimating sediment accumulation rates: Louisiana salt marshes. *Journal of Coastal Research* 11: 296–307.

Morris, James T. 2006. Competition among marsh macrophytes by means of geomorphological displacement in the intertidal zone. *Estuarine, Coastal and Shelf Science* 69: 395–402. https://doi.org/10.1016/j.ecss.2006.05.025.

Morris, James T., Donald C. Barber, John C. Callaway, Randy Chambers, Scott C. Hagen, Charles S. Hopkinson, Beverly J. Johnson, et al. 2016. Contributions of organic and inorganic matter to sediment volume and accretion in tidal wetlands at steady state. *Earth's Future* 4: 110–121. https://doi.org/10.1002/2015EF000334.

Morris, James T., and William B. Bowden. 1986. A Mechanistic, Numerical Model of Sedimentation, Mineralization, and Decomposition for Marsh Sediments. *Soil Science Society of America Journal* 50: 96–105. https://doi.org/10.2136/sssaj1986.03615995005000010019x.

Morris, James T., James Lynch, Katherine A. Renken, Sara Stevens, Megan Tyrrell, and Holly Plaisted. 2020. Tidal and Hurricane Impacts on Saltmarshes in the Northeastern Coastal and Barrier Network: Theory and Empirical Results. *Estuaries and Coasts* 43. Estuaries and Coasts: 1658–1671. https://doi.org/10.1007/s12237-020-00790-5.

Morris, James T., P. V. Sundareshwar, Christopher T. Nietch, Björn Kjerfve, and D. R. Cahoon. 2002. Responses of coastal wetlands to rising sea level. *Ecology* 83: 2869–2877. https://doi.org/10.1890/0012-9658(2002)083[2869:ROCWTR]2.0.CO;2.

Murray, Stephen P., Nan D. Walker, and Charles E. Adams. 1994. *Impacts of Winter Storms on Sediment transport within the Terrebonne Bay Marsh Complex*. Vol. Processes. New Orleans, Louisiana.

Neubauer, S. C., I. C. Anderson, J. A. Constantine, and S. A. Kuehl. 2002. Sediment deposition and accretion in a mid-Atlantic (U.S.A.) tidal freshwater marsh. *Estuarine, Coastal and Shelf Science* 54: 713–727. https://doi.org/10.1006/ecss.2001.0854.

Nolte, S., E. C. Koppenaal, P. Esselink, K. S. Dijkema, M. Schuerch, A. V. De Groot, J. P. Bakker, and S. Temmerman. 2013. Measuring sedimentation in tidal marshes: A review on methods and their applicability in biogeomorphological studies. *Journal of Coastal Conservation* 17: 301–325. https://doi.org/10.1007/s11852-013-0238-3.

Nyman, J. A., R. D. Delaune, and W. H. Patrick. 1990. Wetland soil formation in the rapidly subsiding Mississippi River Deltaic Plain: Mineral and organic matter relationships. *Estuarine, Coastal and Shelf Science* 31: 57–69. https://doi.org/10.1016/0272-7714(90)90028-P.

Nyman, J. A., R. D. Delaune, H. H. Roberts, and W. H. Patrick. 1993. Relationship between vegetation and soil formation in a rapidly submerging coastal marsh. *Marine Ecology Progress Series* 96: 269–279. https://doi.org/10.3354/meps096269.

Nyman, John A., Russel J. Walters, Ronald D. Delaune, and William H. Patrick. 2006. Marsh vertical accretion via vegetative growth. *Estuarine, Coastal and Shelf Science* 69: 370–380. https://doi.org/10.1016/j.ecss.2006.05.041.

Paola, Chris, Robert R. Twilley, Douglas A. Edmonds, Wonsuck Kim, David Mohrig, Gary Parker, Enrica Viparelli, and Vaughan R. Voller. 2011. Natural Processes in Delta Restoration: Application to the Mississippi Delta. *Annual Review of Marine Science* 3: 67–91. https://doi.org/10.1146/annurev-marine-120709-142856.

Parton, W. J., D. S. Schimel, C. V. Cole, and D. S. Ojima. 1987. Analysis of Factors Controlling Soil Organic Matter Levels in Great Plains Grasslands. *Soil Science Society of America Journal* 51: 1173–1179. https://doi.org/10.2136/sssaj1987.03615995005100050015x.

Pennington, W., R. S. Cambray, J. D. Eakins, and D. D. Harkness. 1976. Radionuclide dating of the recent sediments of Blelham Tarn. *Freshwater Biology* 6: 317–331. https://doi.org/10.1111/j.1365-2427.1976.tb01617.x.

Pennington, W., T. G. Tutin, R. S. Cambray, and E. M. Fisher. 1973. Observations on Lake Sediments using Fallout 137Cs as a Tracer. *Nature* 242: 324–326. https://doi.org/https://doi.org/10.1038/242324a0.

Perez, B. C., J. W. Day, L. J. Rouse, R. F. Shaw, and M. Wang. 2000. Influence of Atchafalaya River discharge and winter frontal passage on suspended sediment concentration and flux in Fourleague Bay, Louisiana. *Estuarine, Coastal and Shelf Science* 50: 271–290. https://doi.org/10.1006/ecss.1999.0564.

Restreppo, Giancarlo A., Samuel J. Bentley, Jiaze Wang, and Kehui Xu. 2019. Riverine Sediment Contribution to Distal Deltaic Wetlands: Fourleague Bay, LA. *Estuaries and Coasts* 42. Estuaries and Coasts: 55–67. https://doi.org/10.1007/s12237-018-0453-0.

Rogers, J. D. 2008. Development of the New Orleans Flood Protection System prior to Hurricane Katrina. *Journal of Geotechnical and Geoenvironmental Engineering* 134: 602–617. https://doi.org/10.1061/(asce)1090-0241(2008)134:5(602).

Rovai, Andre S., Robert R. Twilley, Alexandra Christensen, Annabeth McCall, Daniel J. Jensen, Gregg A. Snedden, James T. Morris, and John A. Cavell. 2022. Biomass allocation of tidal freshwater marsh species in response to natural and manipulated hydroperiod in coastal deltaic floodplains. *Estuarine, Coastal and Shelf Science* 268. Elsevier Ltd: 107784. https://doi.org/10.1016/j.ecss.2022.107784.

Rybczyk, J. M., and D. R. Cahoon. 2002. Estimating the potential for submergence for two wetlands in the Mississippi River delta. *Estuaries* 25: 985–998. https://doi.org/10.1007/BF02691346.

Rybczyk, J. 1997. The Use of Secondarily Treated Wastewater Effluent For Forested Wetland Restoration in a Subsiding Coastal Zone. *Dissertation Abstracts International Part B: Science and Engineering* 58: 2896.

Rybczyk, John M., J. C. Callaway, and J. W. Day. 1998. A relative elevation model for a subsiding coastal forested wetland receiving wastewater effluent. *Ecological Modelling* 112: 23–44. https://doi.org/10.1016/S0304-3800(98)00125-2.

Sasser, Charles E., James G. Gosselink, Erick M. Swenson, Christopher M. Swarzenski, and Nancy C. Leibowitz. 1996. Vegetation, substrate and hydrology in floating marshes in the Mississippi river delta plain wetlands, USA. *Vegetatio* 122: 129–142. https://doi.org/10.1007/BF00044695.

Sasser, Charles E., Jenneke M. Visser, Edmond Mouton, Jeb Linscombe, and Steve B. Hartley. 2014. *Vegetation Types in Coastal Louisiana in 2013*. *U.S. Geological Survey*. https://doi.org/10.3133/sim3290.

Schubauer, J. P., and C. S. Hopkinson. 1984. Above- and belowground emergent macrophyte production and turnover in a coastal marsh ecosystem, Georgia. *Limnology and Oceanography* 29: 1052–1065. https://doi.org/10.4319/lo.1984.29.5.1052.

Shaw, John B., Francois Ayoub, Cathleen E. Jones, Michael P. Lamb, Benjamin Holt, R. Wayne Wagner, Thomas S. Coffey, J. Austin Chadwick, and David Mohrig. 2016. Airborne radar imaging of subaqueous channel evolution in Wax Lake Delta, Louisiana, USA. *Geophysical Research Letters* 43: 5035–5042. https://doi.org/10.1002/2016GL068770.

Smalley, Alfred Evans. 1958. The role of two invertebrate populations, Littorina irrorate and Orchelimum fidicinium, in the energy flow of a salt marsh ecosystem. University of Georgia.

Snedden, Gregg A., Kari Cretini, and Brett Patton. 2015. Inundation and salinity impacts to above- and belowground productivity in Spartina patens and Spartina alterniflora in the Mississippi River deltaic plain: Implications for using river diversions as restoration tools. *Ecological Engineering* 81. Elsevier B.V.: 133–139. https://doi.org/10.1016/j.ecoleng.2015.04.035.

Van Soest, P. J. 1963. Use of Detergents in the Analysis of Fibrous Feeds. II. A Rapid Method for the Determination of Fiber and Lignin. *Journal of the Association of Official Agricultural Chemists* 46: 829–835. https://doi.org/10.1007/11679363_33.

Stagg, Camille L., Melissa M. Baustian, Carey L. Perry, Tim J.B. Carruthers, and Courtney T. Hall. 2018. Direct and indirect controls on organic matter decomposition in four coastal wetland communities along a landscape salinity gradient. *Journal of Ecology* 106: 655–670. https://doi.org/10.1111/1365-2745.12901.

Steiger, Johannes, E. Tabacchi, S. Dufour, D. Corenblit, and J. L. Peiry. 2005. Hydrogeomorphic processes affecting riparian habitat within alluvial channel-floodplain river systems: A review for the temperate zone. *River Research and Applications* 21: 719–737. https://doi.org/10.1002/rra.879.

Swanson, Kathleen M., Judith Z. Drexler, David H. Schoellhamer, Karen M. Thorne, Mike L. Casazza, Cory T. Overton, John C. Callaway, and John Y. Takekawa. 2014. Wetland Accretion Rate Model of Ecosystem Resilience (WARMER) and Its Application to Habitat Sustainability for Endangered Species in the San Francisco Estuary. *Estuaries and Coasts* 37: 476–492. https://doi.org/10.1007/s12237-013-9694-0.

Törnqvist, Torbjörn E., Donald R. Cahoon, James T. Morris, and John W. Day. 2021. Coastal Wetland Resilience, Accelerated Sea-Level Rise, and the Importance of Timescale. *AGU Advances* 2: 1–9. https://doi.org/10.1029/2020av000334.

Twilley, R.R., J.W. Day, A.E. Bevington, E. Castañeda-Moya, A Christensen, G Holm, L.R. Heffner, et al. 2019. Ecogeomorphology of coastal deltaic floodplains and estuaries in an active delta: Insights from the Atchafalaya Coastal Basin. *Estuarine, Coastal and Shelf Science*: 106341. https://doi.org/10.1016/j.ecss.2019.106341.

Twilley, Robert R., Samuel J. Bentley, Qin Chen, Douglas A. Edmonds, Scott C. Hagen, Nina S.N. Lam, Clinton S. Willson, et al. 2016. Co-evolution of wetland landscapes, flooding, and human settlement in the Mississippi River Delta Plain. *Sustainability Science* 11. Springer Japan: 711–731. https://doi.org/10.1007/s11625-016-0374-4.

Twilley, Robert R., Lacy R. Blanton, Mark M. Brinson, and Graham J. Davis. 1985. Biomass production and nutrient cycling in aquatic macrophyte communities of the Chowan River, North Carolina. *Aquatic Botany* 22: 231–252. https://doi.org/10.1016/0304-3770(85)90002-6.

Wang, E. C., Tiesong Lu, and W. B. Sikora. 1993. Intertidal marsh suspended sediment transport processes, Terrebonne Bay, Louisiana, USA. *Journal of Coastal Research* 9: 209–220.

Wang, Jiaze, Kehui Xu, Giancarlo A. Restreppo, Samuel J. Bentley, Xuelian Meng, and Xukai Zhang. 2018. The coupling of bay hydrodynamics to sediment transport and its implication in micro-tidal wetland sustainability. *Marine Geology* 405. Elsevier: 68–76. https://doi.org/10.1016/j.margeo.2018.08.005.

Wellner, Robert, Rick Beaubouef, John Van Wagoner, Harry H Roberts, and Tao Sun. 2005. Jet-plume depositional bodies; the primary building blocks of Wax Lake Delta. *Transactions - Gulf Coast Association of Geological Societies* 55: 867–909.

Vita

Amanda Fontenot grew up in the suburbs of Houston, Texas and had an interest for environmental science from an early age. They moved to Louisiana in 2015 to start their undergraduate career at LSU researching wetland soils and getting involved in student government and advocacy. After obtaining a B.S. in Coastal Environmental Science in 2018 with minors in English and Biology, Amanda went on to pursue an Erasmus Mundus Masters in Water Coastal Management. Amanda spent 8 months abroad in Italy, Portugal and Spain learning about integrated coastal zone management practices before returning back to the U.S. when their father fell ill. They started back at LSU in the fall of 2019 in Dr. Twilley's Coastal Systems Ecology Lab and enrolled in the M.S. Coastal and Ecological Engineering program. Their graduate school journey was not an easy one to say the least. Amanda's father, Randolph Andrew Fontenot, passed away in November 2019, four days short of his 57th birthday after a long battle with Multiple Sclerosis and a shorter one with pancreatic cancer. Throughout the past three years, Amanda has survived a global pandemic, flash flooding, mental health struggles, three rounds of COVID-19, and an alligator encounter. However, Amanda also fulfilled some of their dreams during this time by falling in love, adopting their first dog, and getting married in January of 2021. They anticipate graduating in August 2022 with their M.S. in Coastal and Ecological Engineering and pursuing a career in ecological design and coastal engineering. Amanda currently lives in Baton Rouge, LA with their loving spouse – Juni and their two dogs and two cats, and they are excited to continue on a journey of self-discovery outside of school as Andy.